Avalanche Studies and Model Validation in Europe, SATSIE

Ryggfonn measurements Winter 2004/2005

20021048-8 1 December 2005

Client: **European Commission**

Contact person: Denis Peter
Contract reference: Contract of 18.10.02

For the Norwegian Geotechnical Institute

Project Manager: Karstein Lied

Report prepared by: Peter Gauer and Krister Kristensen

Reviewed by: Karstein Lied

Postal address: P.O. Box 3930 Ullevaal Stadion, N-0806 OSLO, NORWAY
Street address: Sognsveien 72, OSLO
Internet: http://www.ngi.no
Telephone: (+47) 22 02 30 00
Telefax: (+47) 22 23 04 48
e -mail: ngi@ngi.no
Postal account: 0814 51 60643
Bank account: 5096 05 01281
Business No. 958 254 318 MVA

SUMMARY

This report presents data collected from the full-scale avalanche test site Ryggfonn during the Winter 2004/2005. The weather and snow conditions are described and when possible, the avalanches have been characterized according to the IAHS avalanche code and the deposit boundaries have been mapped.

Measurements obtained from the avalanche path include impact pressure readings from two load cells at a steel tower as well as impact pressures on three load cells fixed to a concrete structure. In addition, normal stress and shear stress were measured at two locations at a 16 m high dam. Six geophones, placed in the ground in the runout zone, have detected vibrations from some of the passing avalanches. When possible, for each avalanche the front speeds have been estimated. This estimates are based on pulsed Doppler radar measurements, seismic measurements, and the timing between impacts on the constructions. The pulsed Doppler radar provided also velocity measures from the avalanche body.

The measurements obtained are briefly discussed and presented in graphs.

Contents

LIST OF TABLES

LIST OF FIGURES

1 RYGGFONN FULL-SCALE EXPERIMENTS (NGI)

Task leader: Karstein Lied; participation of Krister Kristensen, Carl Harbitz, Peter Gauer, Arne Moe, Erik Lied and Harald Iwe, as well as the Department of Geology and Geophysics, University of Barcelona, the Icelandic Meteorological Office - Avalanche section and Austrian Institute for Avalanche and Torrent Research

1.1 Test site

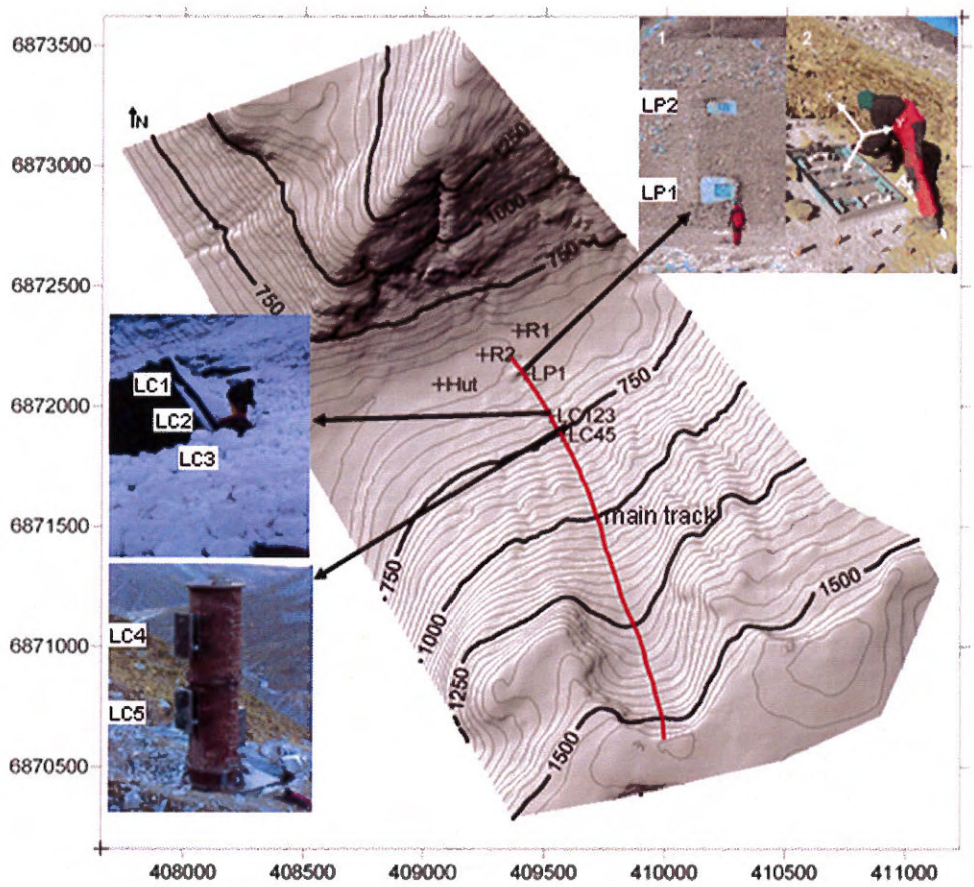

Figure 1.1: Overview of the Ryggfonn test site (UTM coordinates in m). The view shows the line of the main track and the locations of the load cells (LC45 and LC123) and the placement of the load plates in the dam (LP1 and LP2). In addition, two Doppler radar positions are indicated (R1 and R2).

The Ryggfonn full-scale avalanche test site has been in operation since 1980. The test site has a vertical drop of about 900 m and a horizontal length of 2100 m. Typical avalanche

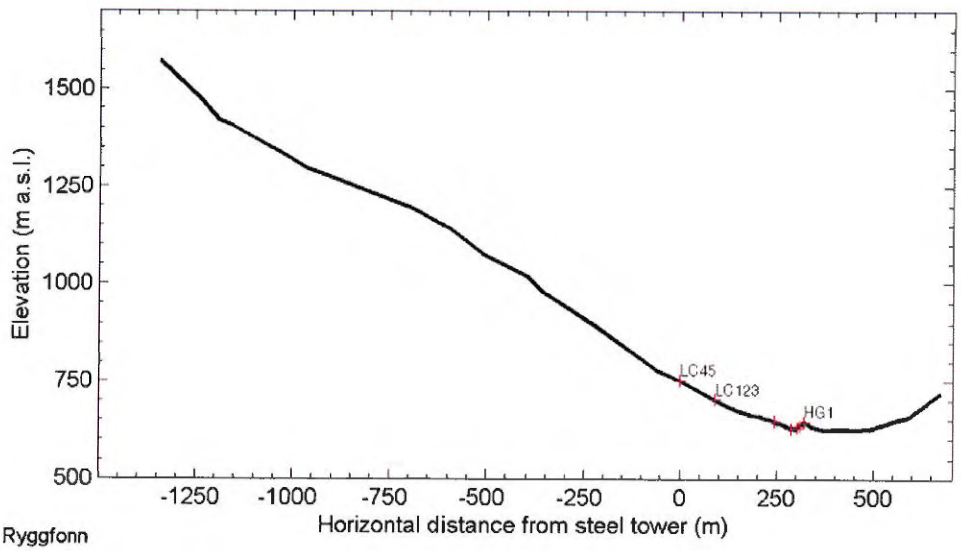

Figure 1.2: Profile line of main track at the Ryggfonn test site. The horizontal distance is measured relative to the steel tower. Sensor positions are indicated

size ranges between 2 (mass of 0.1 Gg) and 4 (mass of 10 Gg) according to the Canadian snow avalanche size classification (McClung and Schaerer, 1993); they may even reach class 5 (mass of 100 Gg). Maximum velocity can reach up to 60 m s^{-1}. Figure 1.1 shows a location map of the main sensors used during the winter season 2004/2005 and Figure 1.2 gives an impression of the profile of the main track.

1.2 Impact pressure measurements

The steel tower has a diameter 1.3 m and is equipped with 2 load plates, each with an area, A_m, of 1.2 m $\times$ 0.6 m. The concrete structure is instrumented with 3 load plates identical to those at the steel tower.

The interpretation of load cell measurements is not straightforward. Commonly, the drag force, F_D, due to a flow around a slender obstacle is expressed in terms of a dimensionless drag factor C_D, i.e.

$$F_D = \frac{1}{2}\rho C_D A_a U_\infty^2 \tag{1.1}$$

Here, ρ is the density of the fluid, U_∞ the upstream flow velocity, and A_a is the projected area of the obstacle that is affected. If A_a is less A_m then the pressure measurements have to be corrected by a (unknown) factor A_m/A_a. This can cause an uncertainty. Reasons for $A_a < A_m$ can be that the flow height of the avalanche is smaller then the height of the plate or the plate is already buried from deposits. The drag factor itself is a function of the

flow regime and depends on factors like the Reynolds number, **Re**, Froude number, **Fr**, and the geometry of the obstacle. If one considers a granular flow, C_D might also depend on the particle concentration, size, and restitution coefficient. Depending on the flow regime, C_D can vary by several orders of magnitude. Despite this, the value used for a rectangular cross section in dry flow avalanches is commonly set to 2, cf. (Mellor, 1968). This holds true for the powder part as well as for the dense part, even if not explicitly stated. In (Norem, 1990), Norem proposed a value of 2.5 for dry snow avalanches and 6.3 for wet snow avalanches based on impact pressure measurements from the Ryggfonn test site. Salm and others (1990) recommend a C_D equals 2 and a density of 300 kg m^{-3}.
Due to the large size of the sensors, the measured impact forces represent average values. Single impacts might exceed these values by an order of magnitude. The averaging effect of the large size also causes a damping of the fluctuation intensity, defined as

$$I_F = \left| \frac{\widetilde{LC} - LC}{\widetilde{LC}} \right| \approx \left| \frac{2u'}{U} + \frac{\rho'}{\rho} \right| \tag{1.2}$$

LC is the measured pressure by the load cell and $\widetilde{LC}$ is a running mean taken either over 0.5 s (approximately between 5 m to 15 m spatial resolution) or 5 m. Temporal averaging has the disadvantage that the spatial resolution might change during time. On the other side, spatial averaging seems only reasonable, if at least a rough estimate of the velocity distribution along the flow direction is available. For a better comparison, the plots of the turbulent intensity are restricted to a maximum value of one, even if partly this value is exceeded. This can occurs mainly in the tail shortly before the avalanche stops and single blocks hit the sensor. In this case the average value is close to zero but the single impact is noticeable.

1.3 Load plate measurements

On the uphill side of the dam, two 1 m^2 large load plates are placed at heights 2 and 8 m above the dam base. The plates are constructed to measure the three stress components: (z) normal to the slope, (x) shear pointing towards the dam crown and (y) shear pointing at a right angle. Each load plate has a maximum measuring range of 400 kPa in the normal direction and 200 kPa for the shear components. A detailed description can be found in (SATSIE, 2003).

In general, an avalanche transmits stresses due to normal pressure, p, and tangential traction, q, at the contact surface. Thus, any stress within a snowpack is a combination of both contributions, and forces measured by a load plate can be written as

$$\begin{aligned} LP_z &= f_z(p, q_x, q_y, \alpha) \\ LP_x &= f_x(p, q_x, q_y, \alpha) \\ LP_y &= f_y(p, q_x, q_y, \alpha) \end{aligned} \tag{1.3}$$

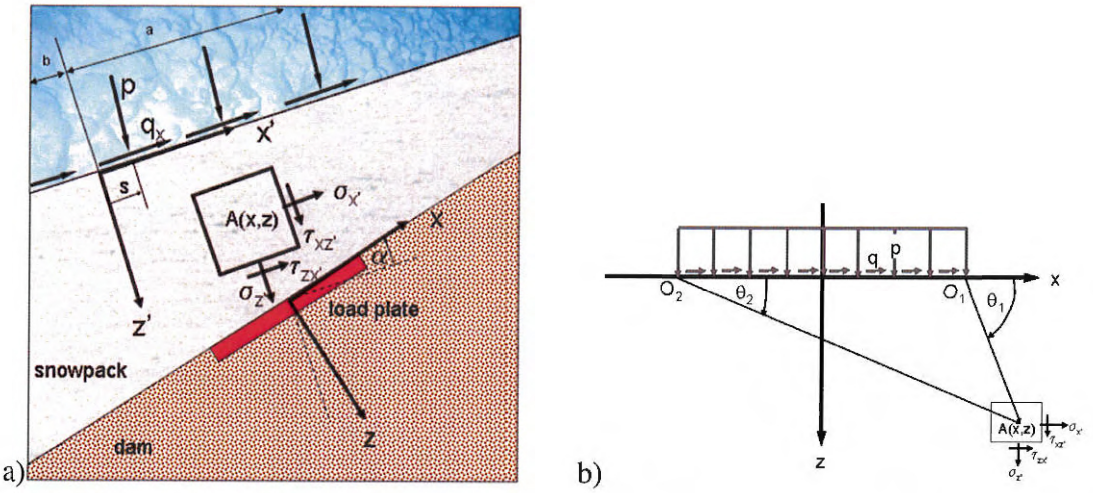

Figure 1.3: Load plate measurements: schematic illustrating the relation between the coordinate systems adapted to the ground and the snow surface, respectively.

where α is the angle between the sliding surface and the plane of the load plate. The functions f_x, f_y, and f_z might be defined using the superposition of the Boussinesq solutions for a point load normal and tangential to the contact surface with an elastic, isotropic and semi infinite medium and their integration over the loaded area. If one assumes, for simplicity, the avalanche as an uniform rectangular load, the measured force can then be used to back-calculate the normal stress, p, and the tangential components, q_x and q_y. Assuming an infinitely wide avalanche hitting the dam and a Poisson ratio ν equal to 0.5, the stresses at a point with coordinates (x,z) (see Fig. 1.3) within the snow pack read

$$\sigma'_x = -\frac{2z}{\pi}\int_{-b}^{a}\frac{p(s)(x-s)^2\,ds}{((x-s)^2+z^2)^2} - \frac{2}{\pi}\int_{-b}^{a}\frac{q_x(s)(x-s)^3\,ds}{((x-s)^2+z^2)^2} \tag{1.4a}$$

$$\sigma'_z = -\frac{2z^3}{\pi}\int_{-b}^{a}\frac{p(s)\,ds}{((x-s)^2+z^2)^2} - \frac{2z^2}{\pi}\int_{-b}^{a}\frac{q_x(s)(x-s)\,ds}{((x-s)^2+z^2)^2} \tag{1.4b}$$

$$\tau'_{xz} = -\frac{2z^2}{\pi}\int_{-b}^{a}\frac{p(s)(x-s)\,ds}{((x-s)^2+z^2)^2} - \frac{2z}{\pi}\int_{-b}^{a}\frac{q_x(s)(x-s)^2\,ds}{((x-s)^2+z^2)^2} \tag{1.4c}$$

The stresses in the system of the load plates are then given by

$$\begin{pmatrix}\sigma_x & \tau_{pxz}\\ \tau_{xz} & \sigma_z\end{pmatrix} = \begin{pmatrix}\cos\alpha & -\sin\alpha\\ \sin\alpha & \cos\alpha\end{pmatrix}\cdot\begin{pmatrix}\sigma'_x & \tau'_{pxz}\\ \tau'_{xz} & \sigma'_z\end{pmatrix}\cdot\begin{pmatrix}\cos\alpha & -\sin\alpha\\ \sin\alpha & \cos\alpha\end{pmatrix}^T \tag{1.5}$$

The angle, α, measure between the dam surface and the surface of the snowpack, depends on the snow distribution in front of the dam. For definition of the load functions in three

dimensions we refer to, e.g., (Johnson, 2001, Chapter 3.2 and 3.6). Due to the motion of the avalanche, the load functions vary with time. Only those parts of the avalanche in proximity to the sensors contribute much as the influence of a distributed load decreases with distance. Shortcomings in the approximations above are: 1) the Poisson ratio, ν, for a real snowpack is less than 0.5; 2) one should consider a layered system consisting of a soft snowpack and a stiffer ground.

1.4 Velocity estimates

Estimates of the avalanche front speed are based on pulsed Doppler radar (DR) measurements by NGI, seismic measurements by the Department of Geology and Geophysics (DGG) at the University of Barcelona, and the timing between impacts on the constructions. In the plot for time series, the zero time is taken as the time when the avalanche hits the first sensor. In the Winter 2004/2005 the first sensor was the steel tower.

Pulsed Doppler radar measurements

In one successful avalanche releases during the season, pulsed Doppler radar systems were used to measure the avalanche velocity. The pulsed Doppler radar emits short pulses and samples the echo in distinct time intervals, corresponding to distance intervals (range gates). Frequency analysis of the echo signals, exploiting the the Doppler effect, yields the velocity distribution within the width of a range gate. Thus, it is possible to gain information on the front speed along the track and information on the velocity versus time at a specific location (Schreiber and others, 2001).
From this information it is also possible to approximately transform times series of measurements at a specific location into a spatial distributions of the same quantity along the avalanche body as it passes the sensor (neglecting any change of the quantity downstream). This allows one to get a glimpse of the spatial structure of the avalanche. The position within the avalanche, x_{pwa}, is a measure of distance behind the front as it is measured by the sensor after a given time. The position can be calculated by

$$x_{pwa} = \int_{t_0}^{t} u(t)\, dt \tag{1.6}$$

where t_0 is the arrival time of the front at the specific location. x_{pwa} is comparable to the wind run used in meteorology.

In addition to the velocity, information on accelerations can be derived. To this end, the velocities of a pair of adjoining range gates, having a width Δx are compared. Starting with a first guess of the average velocity, $\overline{u}$, between both range gates (either the upstream velocity, $u_1(t_1)$, or another suitable estimate) the required travel time, $\Delta t = \Delta x/\overline{u}$, between the range gates can be calculated. Then, the velocity of the downhill range gate $u_2(t_1 + \Delta t)$ is used to recalculate $\overline{u} = (u_1(t_1) + u_2(t_1 + \Delta t))/2$. In this way, the average velocity can be found iteratively. The estimated acceleration is calculated by

$$a = \frac{(u_1(t_1) - u_2(t_1 + \Delta t))}{\Delta t} \tag{1.7}$$

However, one should keep in mind that the measured velocities are actually only a weighted average speed within the width of the range gate. In the experiments, range gate widths of 25 m, were used.

Commonly used model equations for avalanches base the balance between driving force due to gravity and the resisting force due to dry friction (no velocity dependency) and friction which is linear and quadratic in the velocity (cf. Mellor (1968)). This can be written by

$$a = g \sin\phi - (a_0 cos\phi + a_1 u + a_2 u^2) \tag{1.8}$$

Using the calculated acceleration (deceleration) values from (1.7), it is possible to fit these according to (1.8) and so gain some idea of the friction coefficients. It should be noted that a_1 and a_2 in this representation are function of the flow height. Not included in this approximation are effects due to the gradient of the normal pressure appearing in models based on continuum mechanics.

2 WINTER 2004/2005

2.1 General conditions in 2004/2005

The first part of the 2004-2005 was fairly stormy with comparatively large amounts of snow. By the end of January the total snow height at 930 m a.s.l. was 340 cm, corresponding to more than 200% of the median for this month. The winds in this period had a slightly more westerly component than normal, which resulted in a rather unusual snow deposition pattern, and as an effect of this, avalanche releases at unusual locations. This is reflected in the release pattern of the winter's largest avalanche in Ryggfonn in early January.

The snow was nevertheless mostly stable during the winter, except for a depth hoar layer near the ground that had been established in December. This situation caused unexpected avalanching in some paths, but the January avalanche in Ryggfonn resolved the situation in this starting zone.

Due to the loss of the meteorological station at Fonnbu by fire, no monthly climate data are available. However, Fig. 2.1 shows weather measurements from stations close to the avalanche site. Red line graphs indicate measurements made in the runout zone at 600 m a.s.l., blue graphs indicate indicate measurements made at a ridge station close to the starting zone at 1400 m a.s.l. The precipitation is measured at a valley station (Sindre, Stryn). The vertical lines are the avalanche occurrences in the Ryggfonn path.
The following avalanches were observed in the Ryggfonn path this winter:

- December 7 2004 at 17:00 h: naturally released small avalanche
- January 7 2005 at 04:16 h: naturally released wet snow avalanche; this avalanche consisted mostly likely of two distinguish surges of which the first surge was a dry mixed avalanche and the second more wet.
- April 15 2005: naturally released small dry snow avalanche
- April 16 2005 at 15:00 h: artificially released dry snow avalanche

A classification is given in Tab. 2.1 and an overview of the available measurements in Tab. 2.2. Figure 2.2 plots the outlines of the two major avalanches at Ryggfonn in Winter 2004/2005.

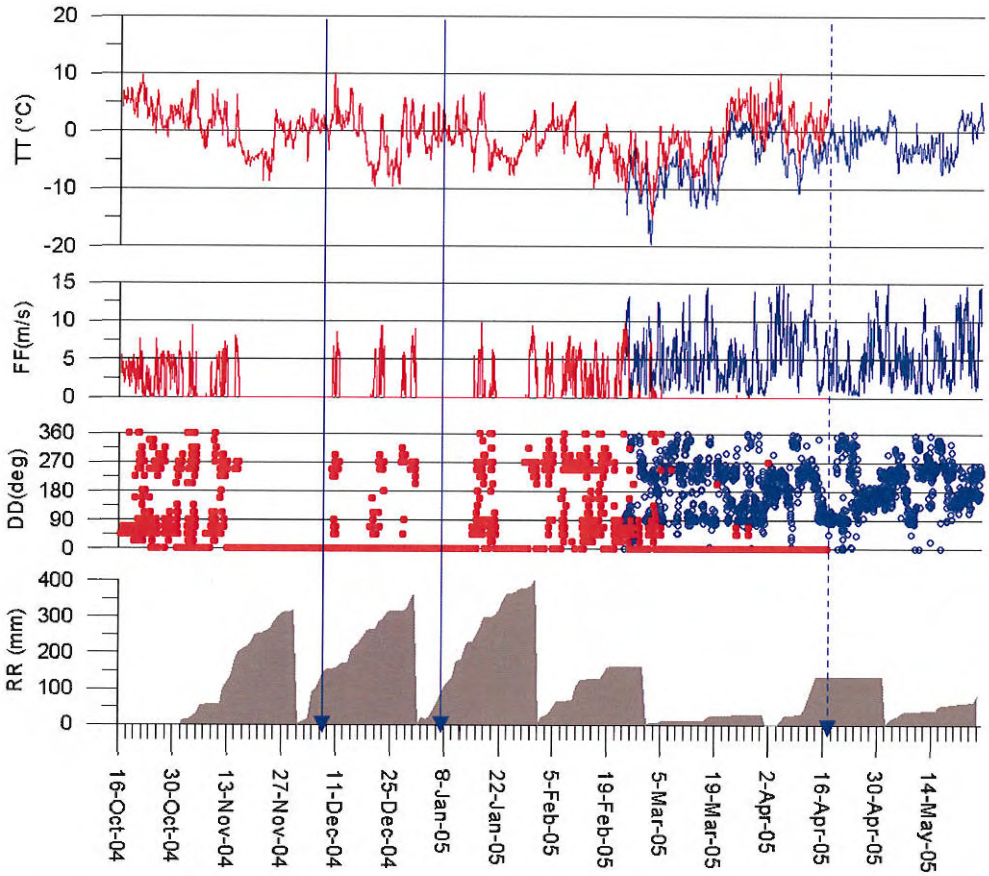

Figure 2.1: Weather data from Ryggfonn test site. Red line graphs indicate measurements made in the runout zone at 600 m a.s.l., blue graphs indicate indicate measurements made at a ridge station close to the starting zone at 1400 m a.s.l. The snow height and the unfilled accumulated precipitation graphs is based on data from the DNMI-station 58880 Sindre, 118 m a.s.l. Vertical lines with arrows indicate avalanches in Ryggfonn (solid=natural, dotted=artificial avalanche)

Table 2.1: Avalanche classification

Date yyyymmdd hh:mm	Size[1]	Deposit (10^3 m^3)	Classification (ICSI)[2] A	B	C	D	E	F	G	H	J	Speed (m s^{-1}) LC4–LC1[3] 101 m	LC1–LP1[4] 218 m
20041207 17:00	NA	NA	3	2	1	2	7	3	2	1	1	NA	NA
20050107 04:16	4	NA	3	2	1	1	7	3	2	1	1	30	17
20050107 04:16 b	4	NA	3	2	1	1	2	3	2	1	1	NA	5
20050415	NA	NA	7	/	1	2	/	/	1	1	1	NA	NA
20050416 15:00	4	NA	4	7	1	2	7(2)	2	7	3	4	30	5

[1]According to Canadian avalanche size classification, cf. (McClung and Schaerer, 1993)
[2]According to International Avalanche Classification (Avalanche Atlas (UNESCO, 1981), also in (McClung and Schaerer, 1993))
[3]The estimated average speeds are calculated between the steel tower and the concrete structure,
[4]and between the concrete structure and the foot of the dam, respectively.

Table 2.2: Overview of archived measurements at Ryggfonn test site during winter season 2004/2005

Date yyyymmdd hh:mm	geophone (GF)1 2 3 4 5 6 H1	load cell (LC)4 5 1 2 3	load plate (LP)1 2	radar P-DR	field obs.	maps
20041207 17:00	X O O O O O O	U X O O O	O O	–	–	X
20050107 04:16	X X X X X X X	X X X X X	X X	–	–	X
20050107 04:16 b						
20050415	– – – – – – –	– – – – –	– –	–	–	X
20050416 15:00	X X X X X X X	B X X X X	X X	X	X	X

Codes: X -data; P -sensor partly buried; B -sensor buried; O -data, but no measured signal (did not reach sensor); – -no data; U sensor status unknown

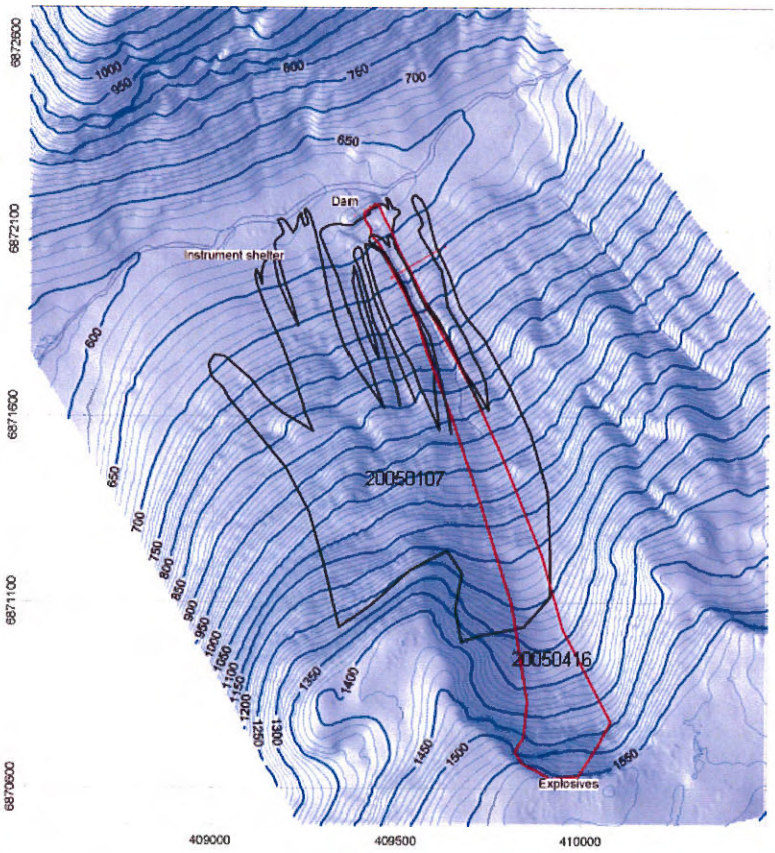

Figure 2.2: Map of the Ryggfonn test site with the all avalanche deposits recorded in Winter 2004/2005. The black line indicates the natural avalanches, while the red solid line represents an artificially released avalanche on 20050416 15:00

2.2 Avalanche 20041207 17:00

Avalanche code (UNESCO/IAHS 1981): A3, B2, C1, D2, E7, F3, G2, H1, J1.

Weather and avalanche summary At 930 m a.s.l., the air temperature was -0.7°C, with high temperatures of 4.0°C the preceding 24 hours. At the time of the avalanche release there were SSW-wind of 6 m s^{-1}, with gusts up to 12 m s^{-1}. In the runout zone at 600 m a.s.l. the temperature was 2.7°C, which was also the highest in the preceding 24 hour period.

Results

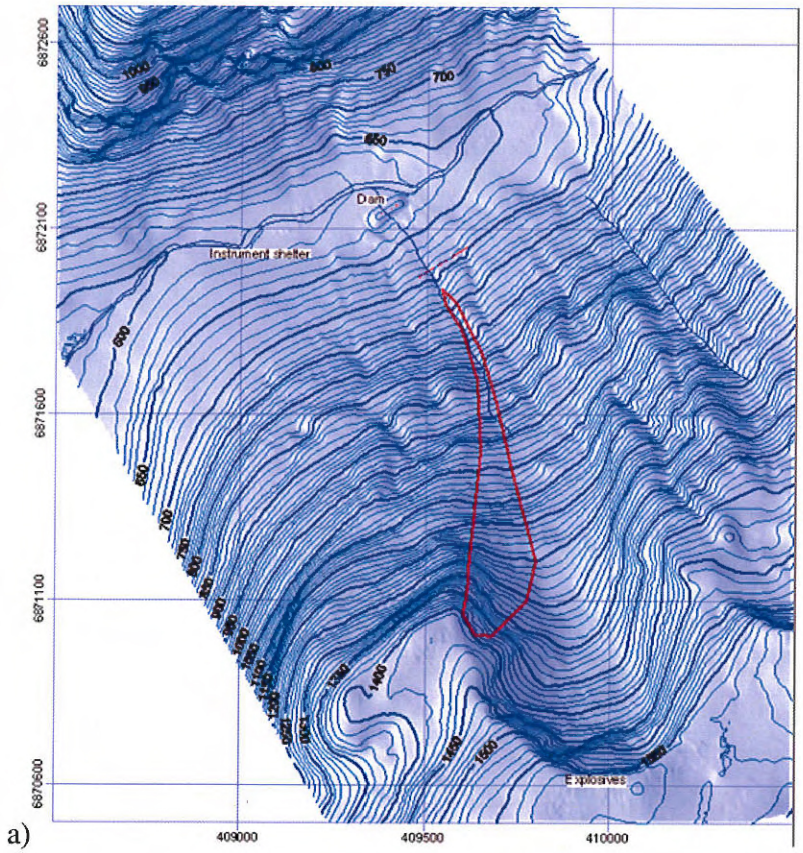

Figure 2.3: Avalanche 20041207 17:00: Deposition/outline map.

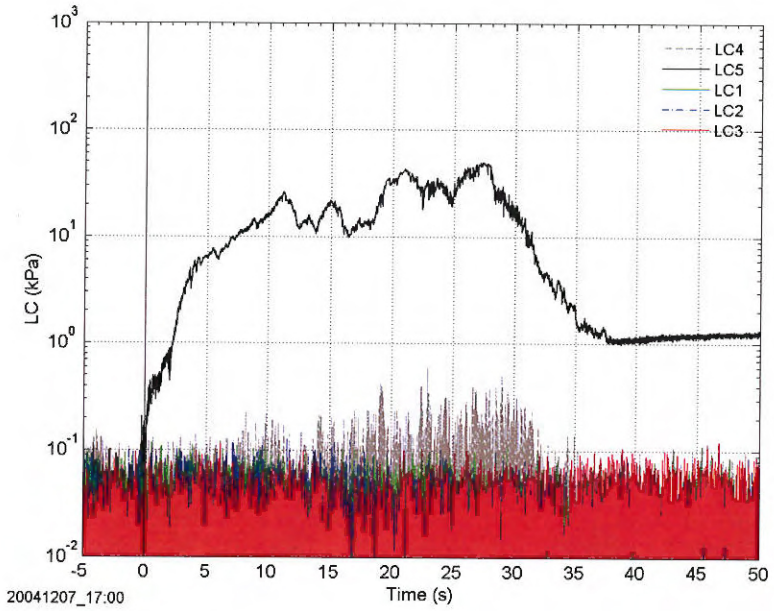

a)

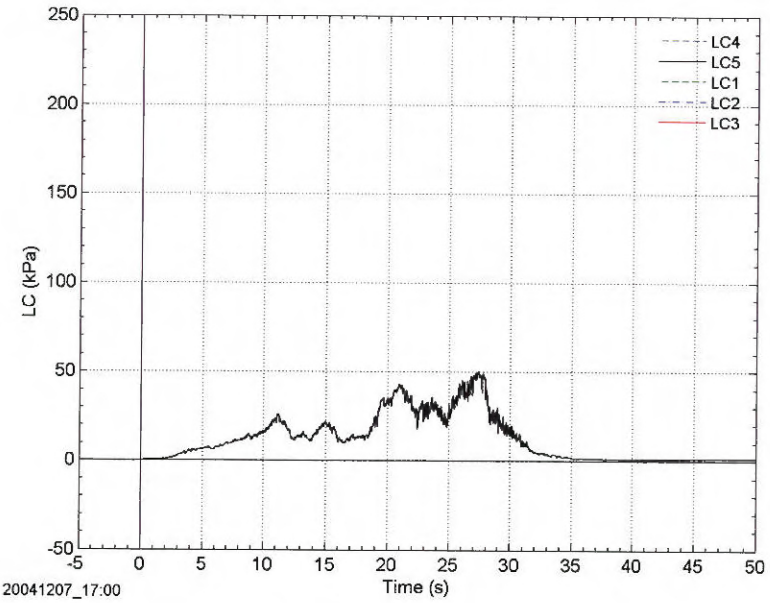

b)

Figure 2.4: Avalanche 20041207 17:00: Load cell measurements: pressure vs. time; a) logarithmic and b) linear presentation.

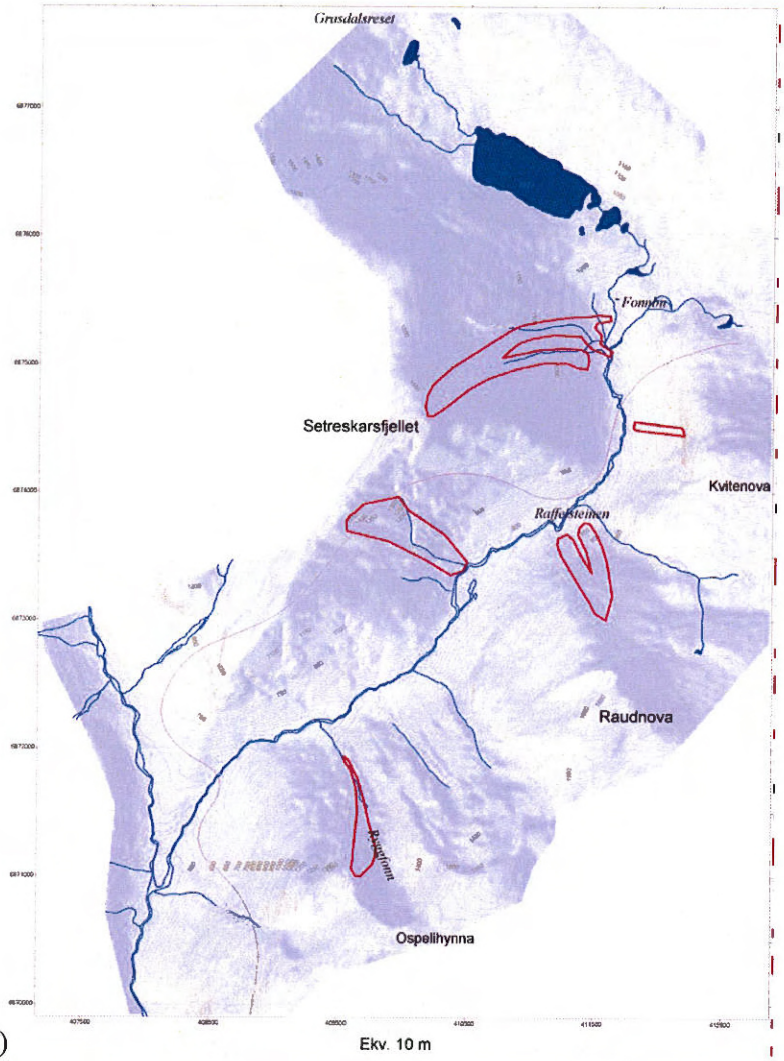

a)

b)

Figure 2.5: Avalanche 20041207 17:00: Deposition/outline map in the Ryggfonn area (upper panel); Avalanche deposit in the Fonnbu area around the same time (lower panel).

2.3 Avalanche 20050107 04:16

Avalanche code (UNESCO/IAHS 1981): A3, B2, C1, D1(2), E7, F3, G2, H1, J1.
(second avalanche A3, B2, C1, D1(2), E2, F3, G2, H1, J1).

During a period of strong winds and snow in the first part of January, several natural avalanches ran in the Ryggfonn path and the adjacent area. Because the 0°C isotherm was at around 1000 m a.s.l. at the time of release, the avalanche consisted of partly wet snow. As can be seen from the map, the avalanche originated from the west side of the cirque and lower on the west ridge. Bad visibility and irregular terrain made it difficult to estimate the depth and extent of the initial fracture.

Weather and avalanche summary At the time of the avalanche release at 04:16 h, the air temperature at 930 m a.s.l. was -0.1°C, with high temperatures of 0.8°C the preceding 5 hours. There were strong winds from SSW, with gusts up to 19 $m\,s^{-1}$, heavy snowfall and drifting snow in the starting zone. In the runout zone at 600 m a.s.l. the temperature was 0.4°C, with high as 3.5°C, four hours earlier.

Results

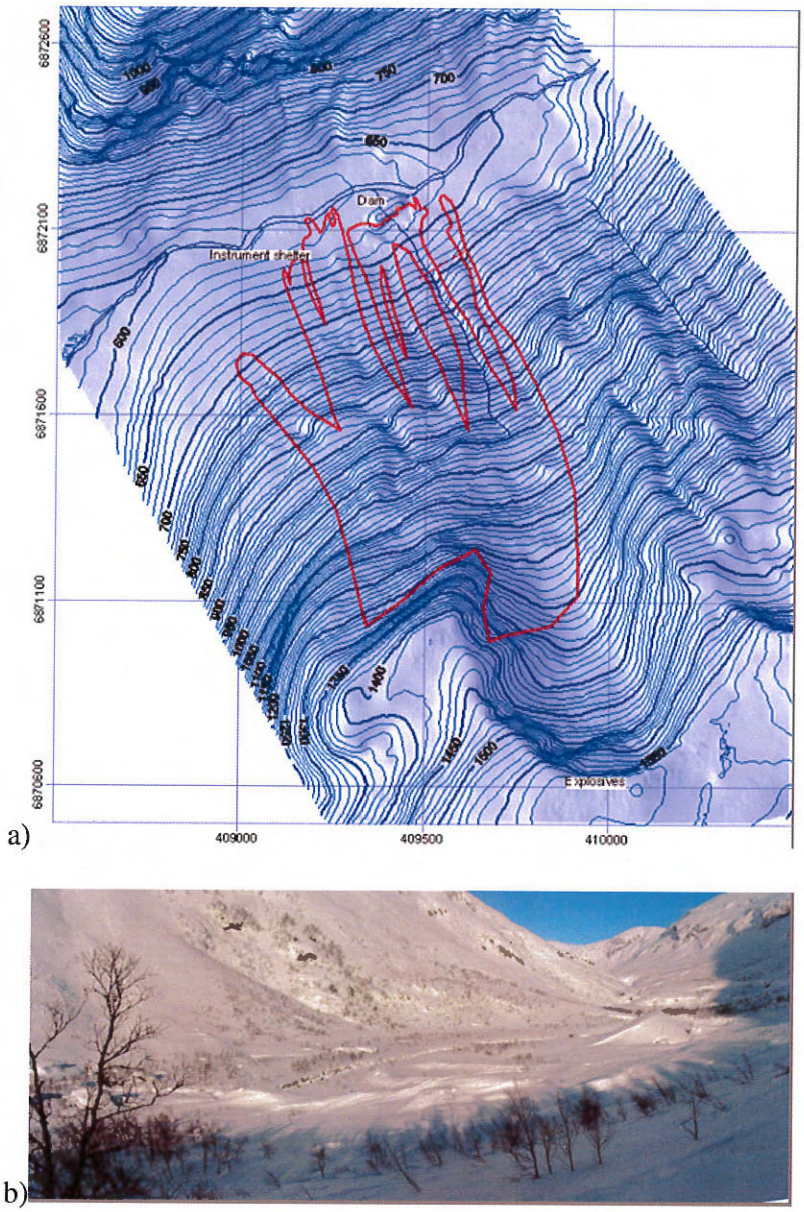

Figure 2.6: Avalanche 20050107 04:16: Deposition/outline map (upper panel); area of the dam after the avalanche.

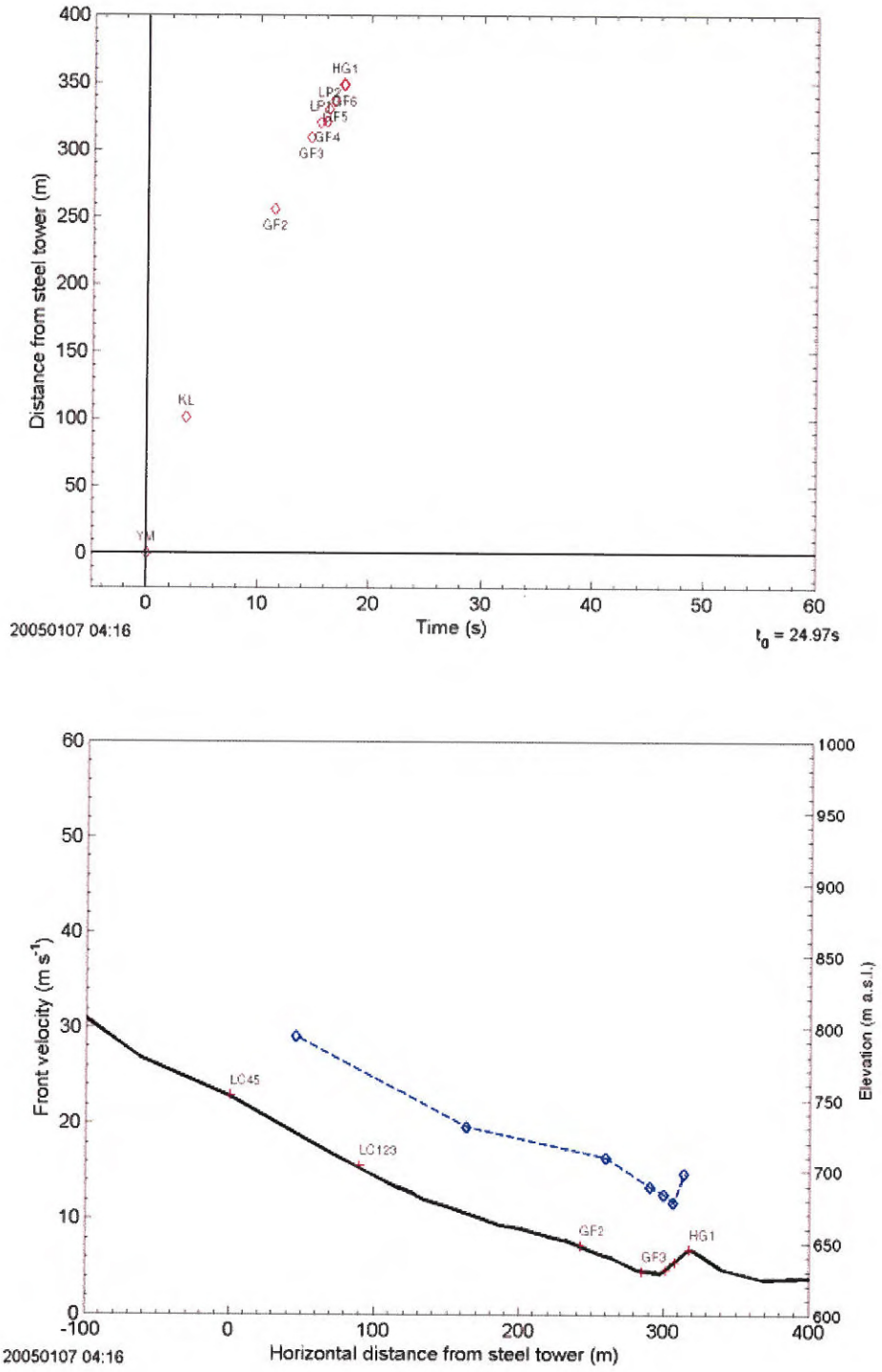

Figure 2.7: Avalanche 20050107 04:16: Timing of the first surge; Distance vs. time (top); Front velocity vs. horizontal distance (bottom). Shown are estimates based on the arrival times at various sensor locations.

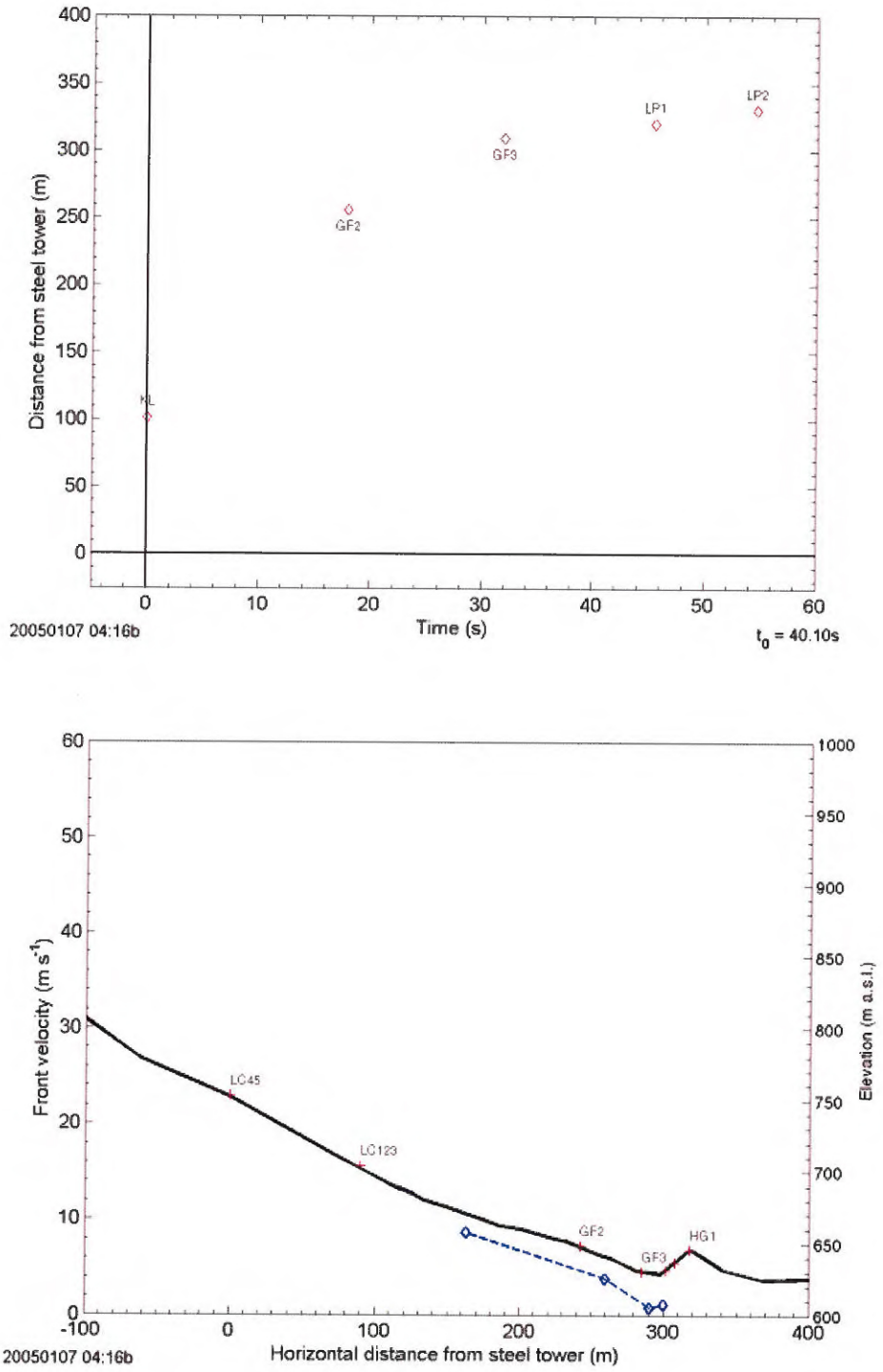

Figure 2.8: Avalanche 20050107 04:16: Timing of the first surge; Distance vs. time (top); Front velocity vs. horizontal distance (bottom). Shown are estimates based on the arrival times at various sensor locations.

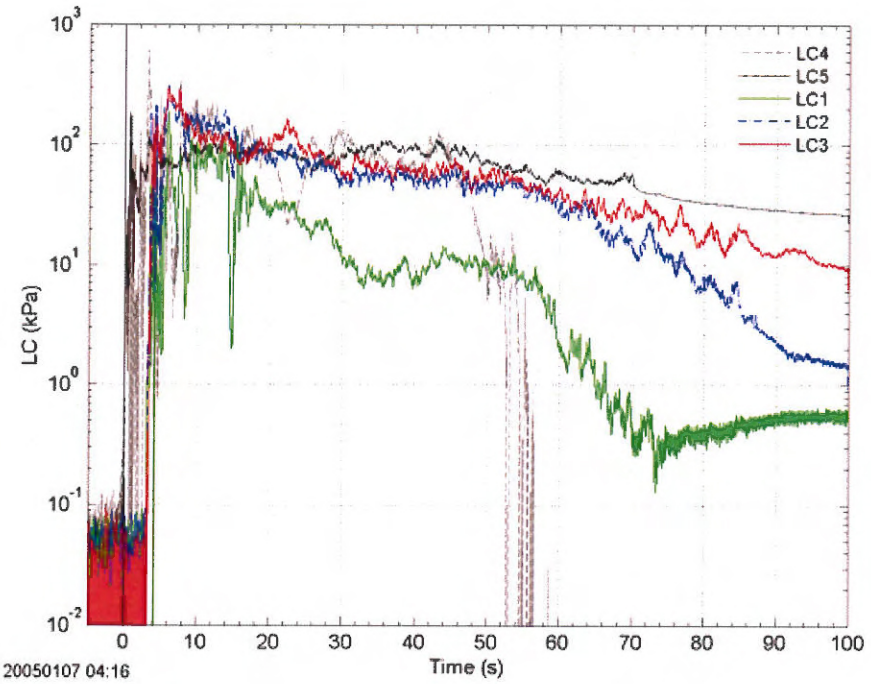

a)

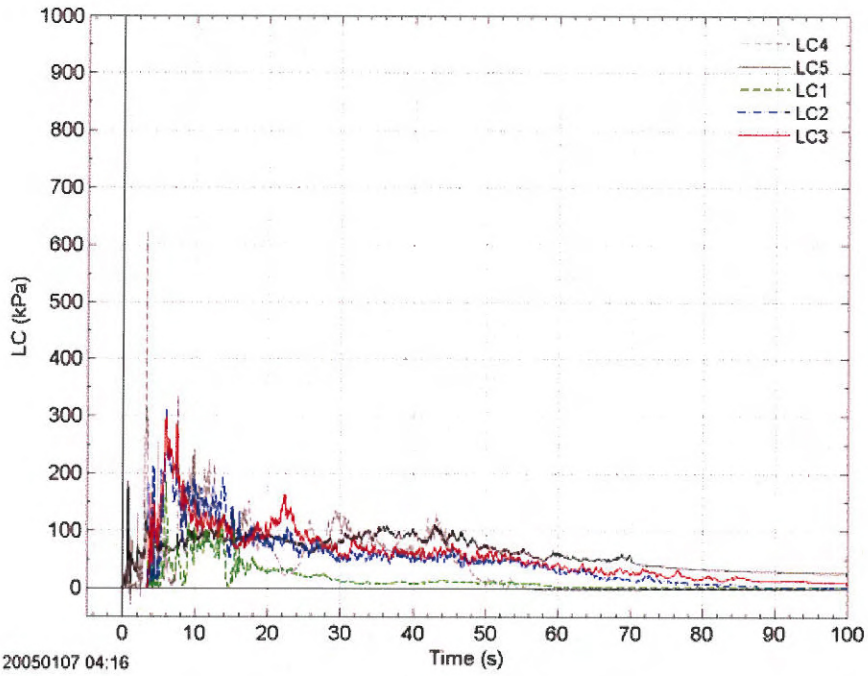

b)

Figure 2.9: Avalanche 20050107 04:16: Load cell measurements (raw data): pressure vs. time; a) logarithmic and b)linear presentation.

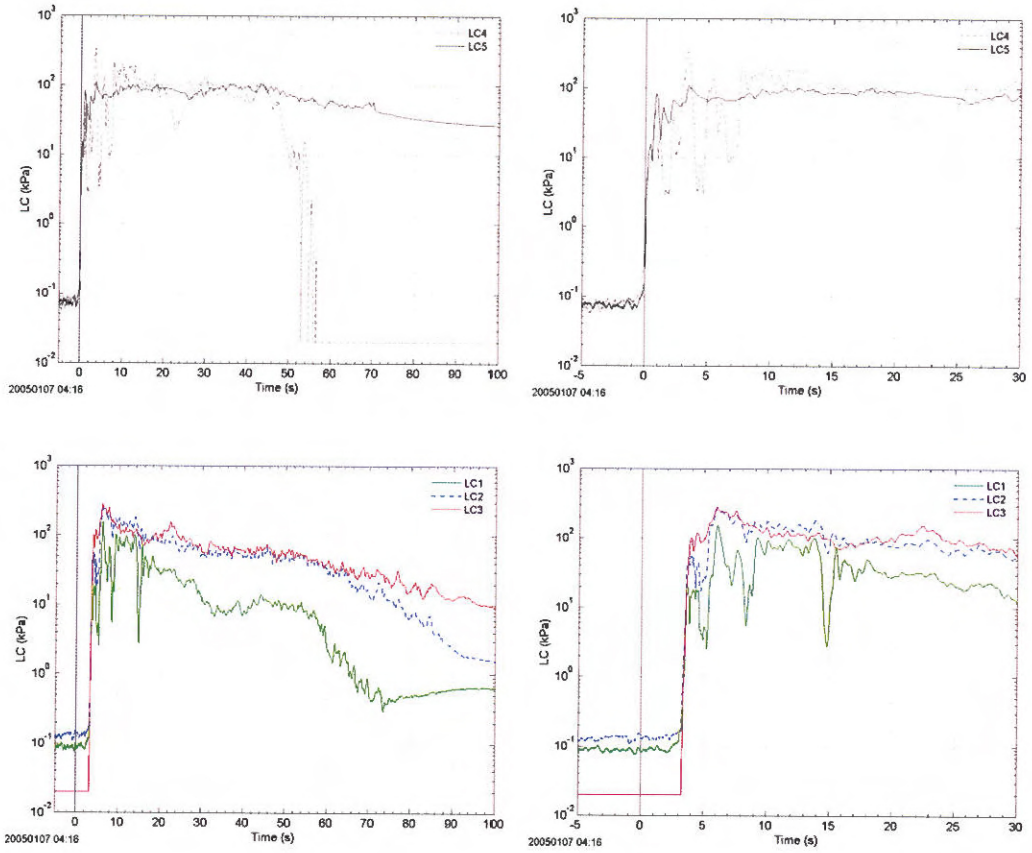

Figure 2.10: Avalanche 20050107 04:16: Load cell measurements: pressure vs. time; top) at the steel tower; and bottom) at the concrete wedge. Data are running means over 0.25 s. Right hand shows an enlargement of the first 30 s.

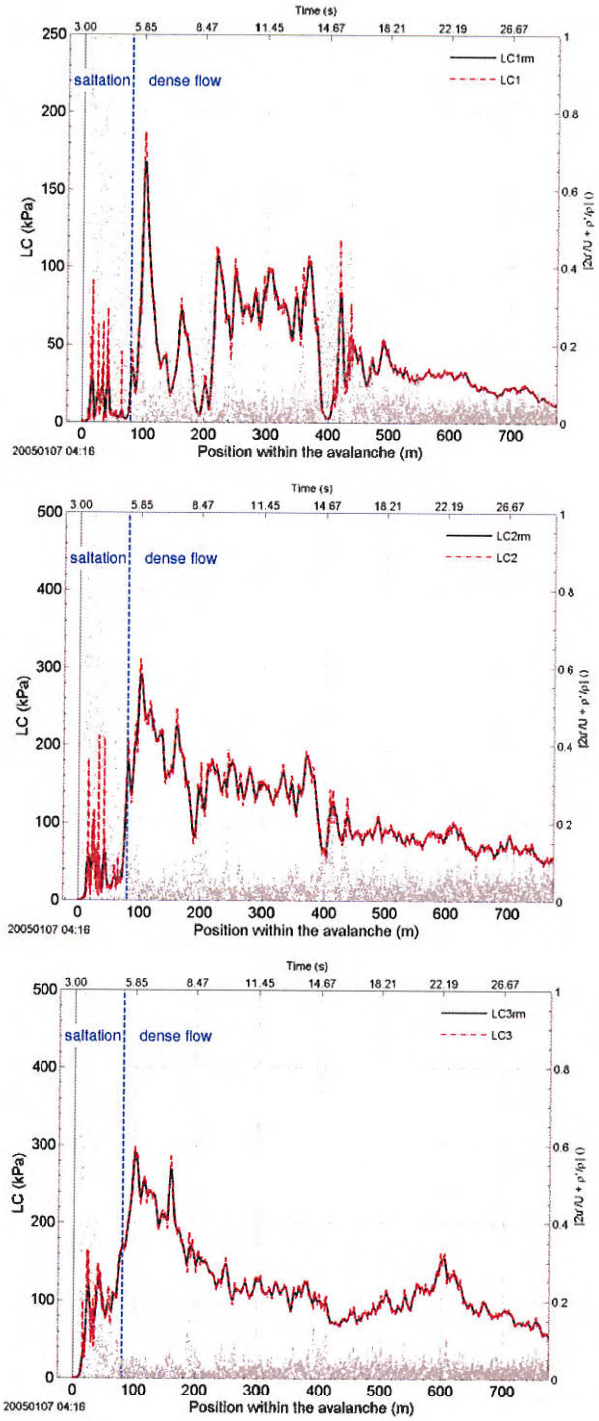

Figure 2.11: Avalanche 20050107 04:16: Fluctuation intensity vs. position within the avalanche. The lines present the measured impact pressure (dashed line) and the running mean (full line) taken over 5 m, respectively (left axis), at the concrete wedge. The fluctuation intensity is marked with dots (right axis). The underlying velocity profile is based on correlation between pressure measurements at the steel tower and the concrete wedge and should be regarded as a rough estimate. Top: LC1; middle: LC2; bottom LC3.

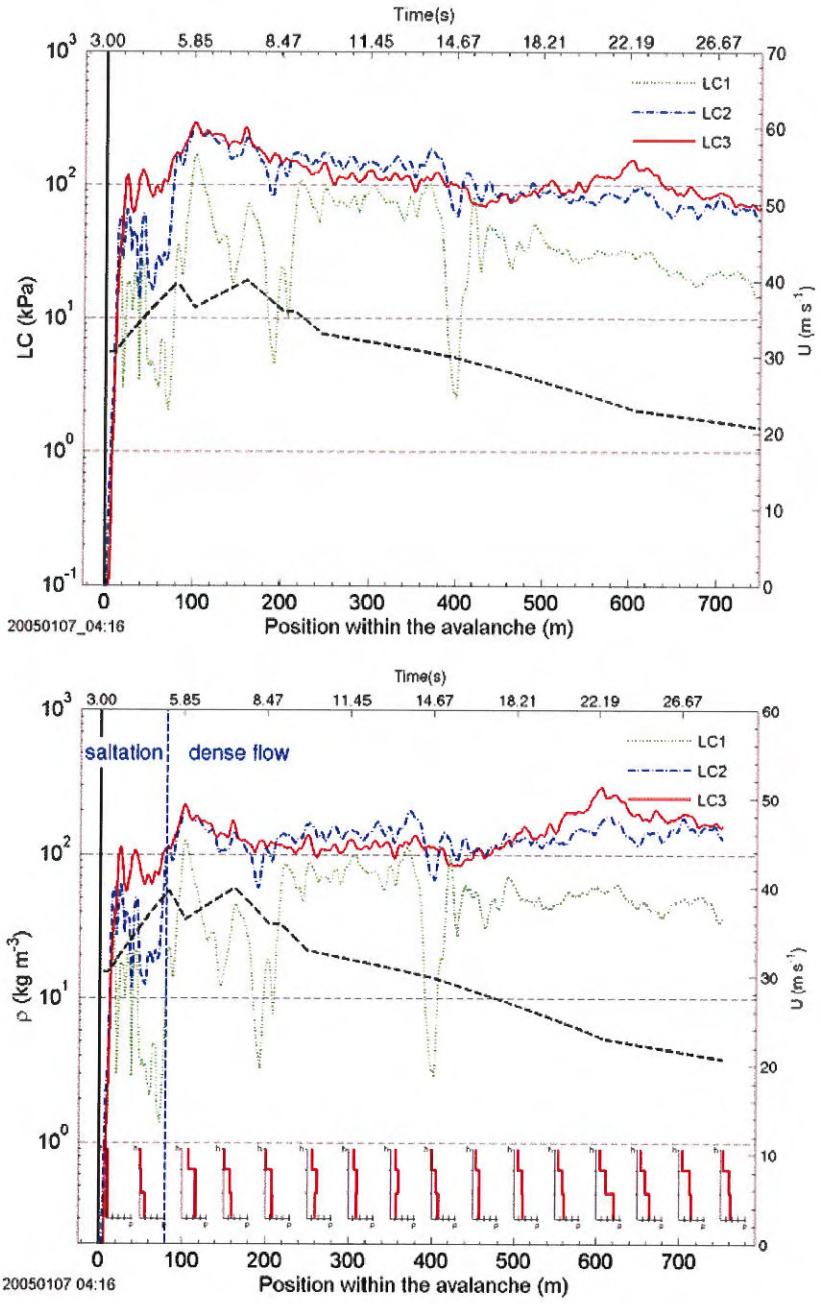

Figure 2.12: Avalanche 20050107 04:16: Impact Pressure vs. position within the avalanche (top). Estimated density vs. position within the avalanche assuming $C_D \approx 2$ (bottom). Data are running means taken over 5 m. Note the logarithmic scaling of the left ordinate and the different horizontal scaling. The small inset profiles indicate the vertical density distribution showing the mean density over the height of individual plates (ticks mark density steps by 100 kg m^{-3}). The black line shows the corresponding velocity profile (right axis). The underlying velocity profile is based on correlation between pressure measurements at the steel tower and the concrete wedge and should be regarded as a rough estimate. Correlation between LC4 and LC1 might indicate higher velocity in the frontal part.

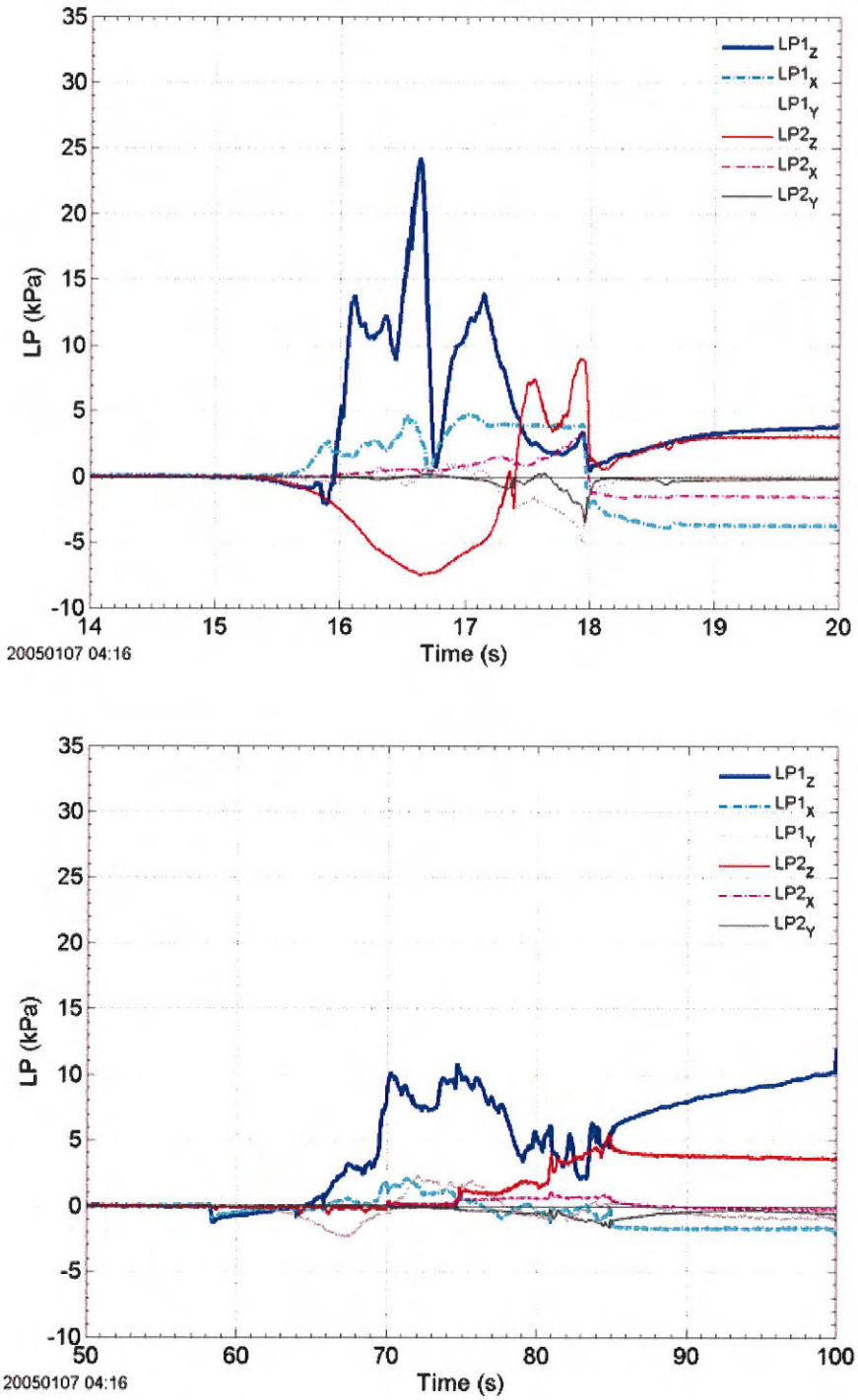

Figure 2.13: Avalanche 20050107 04:16: Load plate measurements: LP (raw data) vs. time. Top: first surge; bottom: second surge

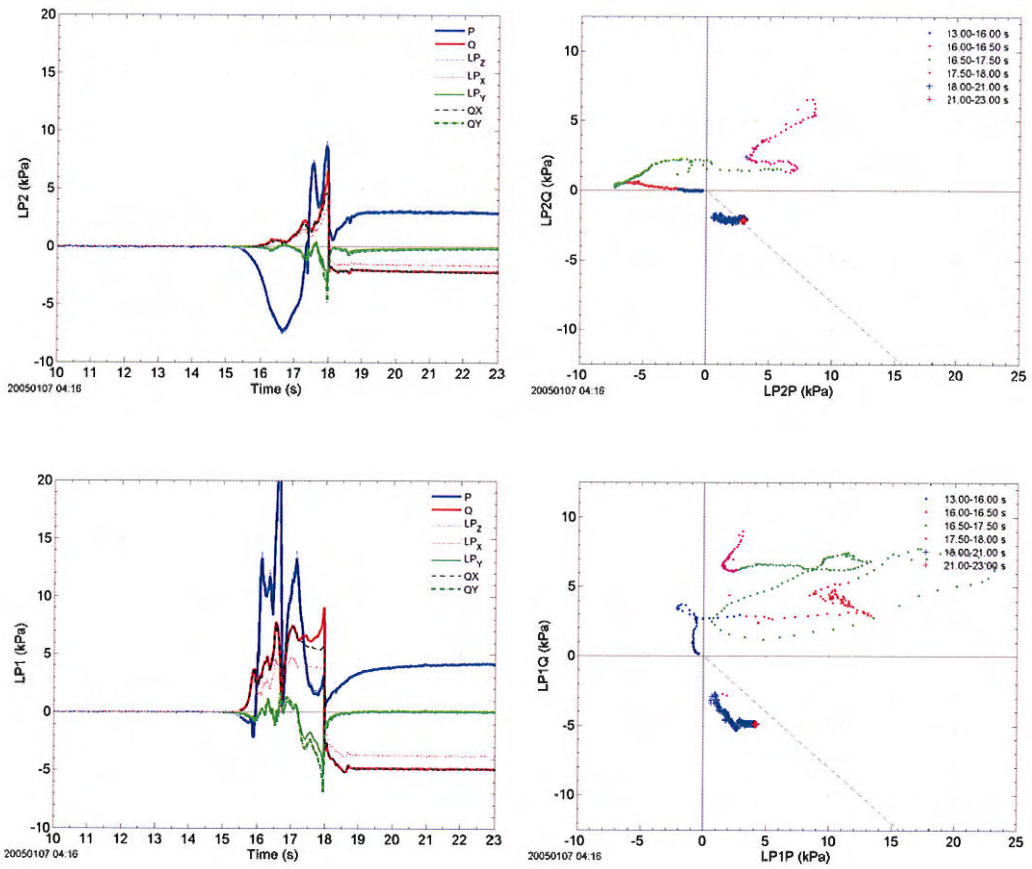

Figure 2.14: Avalanche 20050107 04:16: Load plate measurements; first surge: Stresses vs. time (left hand side) and shear stress vs. normal stress at the sliding plane (surface of the snowpack) along the dam slope (right hand side). The upper panel shows LP2 and the lower one LP1. LP_z and LP_x mark the measured stresses. P and Q are the calculated stresses according to (1.3). The dashed line in right panels corresponds to the ratio between shear and normal stress in the case of static loading ($-\tan 20°$ or $-\tan 40°$).

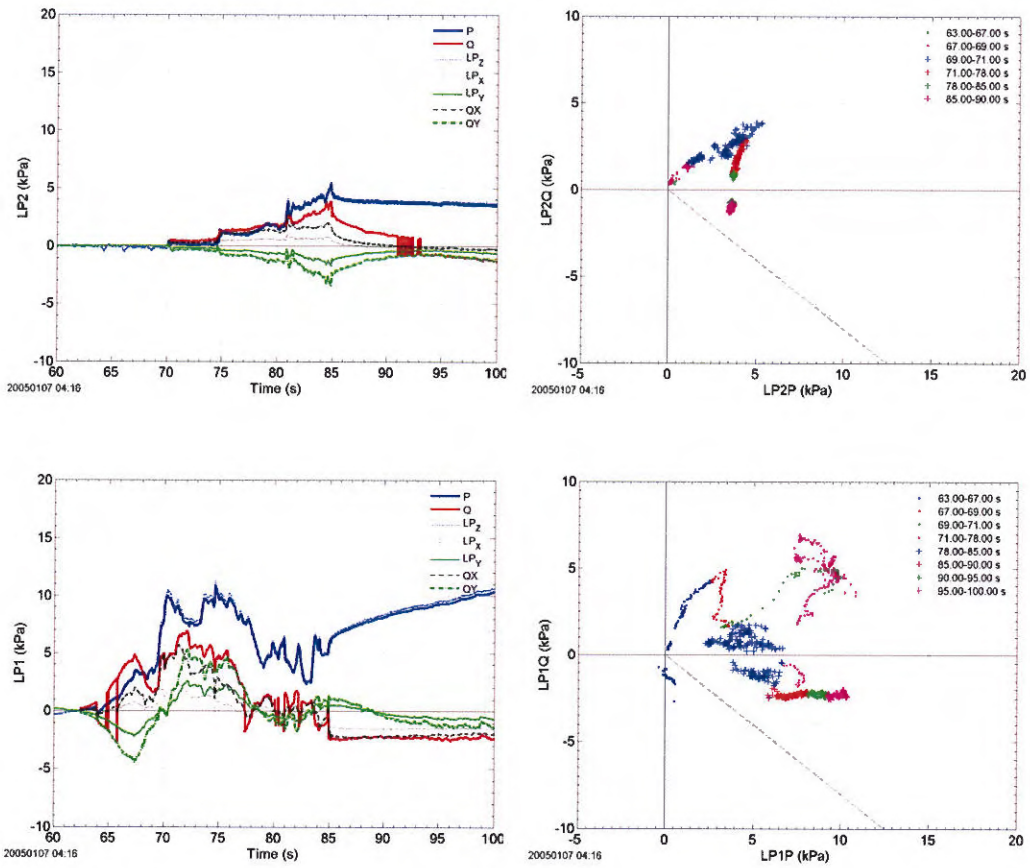

Figure 2.15: Avalanche 20050107 04:16: Load plate measurements; second surge: Stresses vs. time (left hand side) and shear stress vs. normal stress at the sliding plane (surface of the snowpack) along the dam slope (right hand side). The upper panel shows LP2 and the lower one LP1. LP_z and LP_x mark the measured stresses. P, and Q are the calculated stresses according to (1.3). The dashed line in right panels corresponds to the ratio between shear and normal stress in the case of static loading $(-\tan 40°)$.

2.4 Avalanche 20050416 15:00

Avalanche code (UNESCO/IAHS 1981): A4, B2, C1, D2, E7(2), F3, G7, H3, J4.

After nearly two months of stable weather and snow conditions there was a period of snowfall and SW winds in the first part of April. It was decided to attempt a blasting of Ryggfonn when the weather cleared around the 15th. Before the blasting could be done however, a small avalanche ran in the lower path as a result of afternoon sunshine on the 15th. On the 16th the main Ryggfonn avalanche was released by detonating 150 kg of explosives buried in the top cornice

Weather and avalanche summary Sunny and calm with 25 cm fresh snow deposition from previous days. At 1420 m a.s.l the air temperature was -2.5°C, with high temperatures of -1.5°C the preceding 24 hours. SW-wind of 2 $m\,s^{-1}$, with gusts up to 5 $m\,s^{-1}$. In the runout zone the temperature was 5.1°C at the time of release.

Results

Figure 2.16: Avalanche 20050416 15:00: Snapshot from the avalanche release (photo by L. Rammer).

Figure 2.17: Avalanche 20050416 15:00: Snapshot from avalanche descent taken from the video by K. Kristensen.

Table 2.3: Field observations/ measurements

location	clod density ($kg\,m^{-3}$)	snow temperature (°C)	water content	comments
by the dam	450	-5		
	530			
by the dam	450	0	wet	surrounding snowpack
	450	0		
	650	-5	dry	
	670	0	wet	
	650	0	wet	
	450	-4	dry	
	600	0	wet	
50 m above the dam	450	-5	dry	
	450	-5	dry	
	350	-5	dry	
	380	-5	dry	
	570	0	wet	within shear plane
75 m above the dam	500	-5	dry	
at the concrete wedge	400	0	wet	shear plane 25 m west
	500	0	wet	shear plan 10 m west 1 1/2 plates visible, wedge of avalanche snow in front of the plates 40 cm edge length west 70 cm edge length east
at the steel tower	600	0		at the plate wedge of avalanche snow in front of the plates 80 cm edge length west 5 m length; 2–3 m width
	670	0		clod size: 0.1–0.5 m
	690	0		
	400	0		
	660	0		
	630	0		

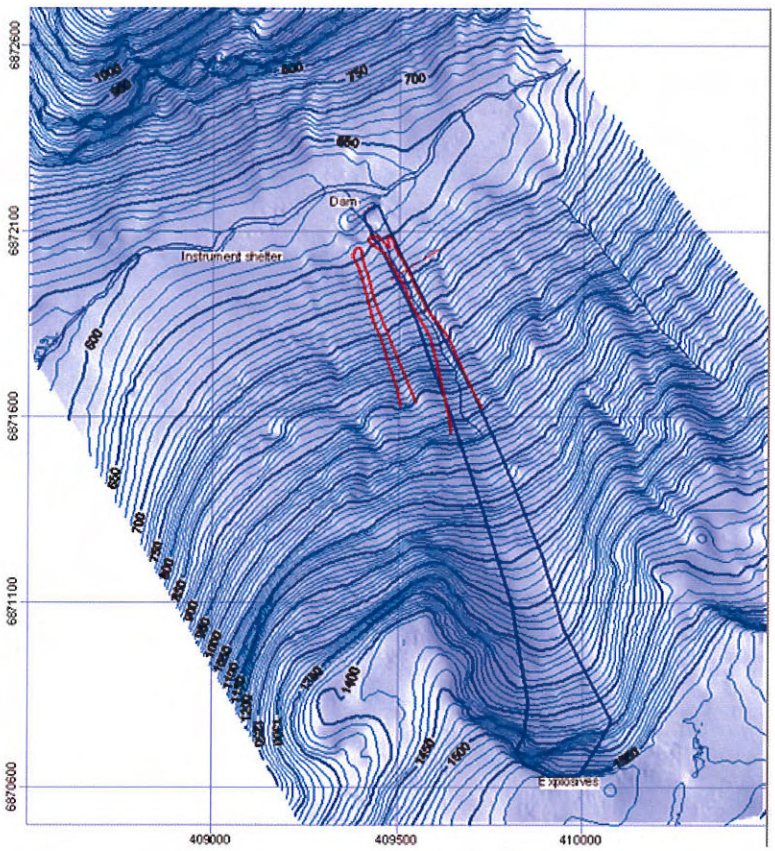

Figure 2.18: Avalanche 20050416 15:00: Deposition/outline map. Red lines events 20050415; blue line 20050416 15:00

Figure 2.19: Avalanche 20050416 15:00: Track status before the event. (Photos by Arne Moe)

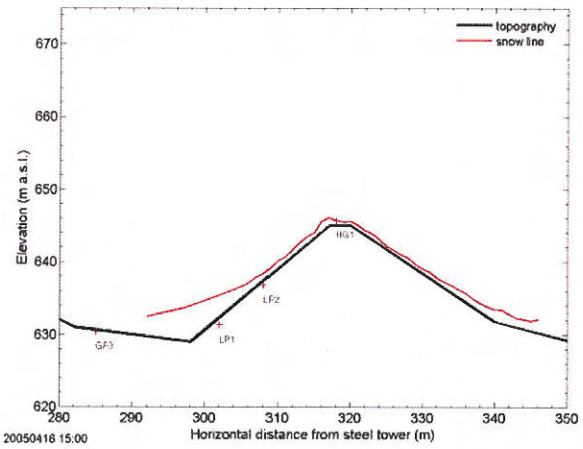

Figure 2.20: Avalanche 20050416 15:00: Snow depth profile at the dam before the event.

Figure 2.21: Avalanche 20050416 15:00: Sensor status before and after the event. Top: load cells at the steel tower; bottom at the concrete wedge. (Photos by Karstein Lied and Peter Gauer)

Figure 2.22: Avalanche 20050416 15:00: Sensor status after the event; the width of concrete wedge is about 0.6 m. (Photo by Krister Kristensen)

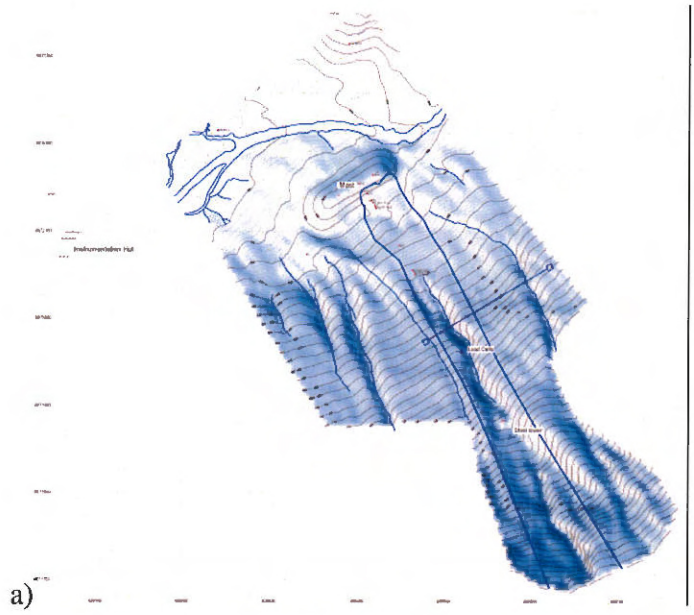

a)

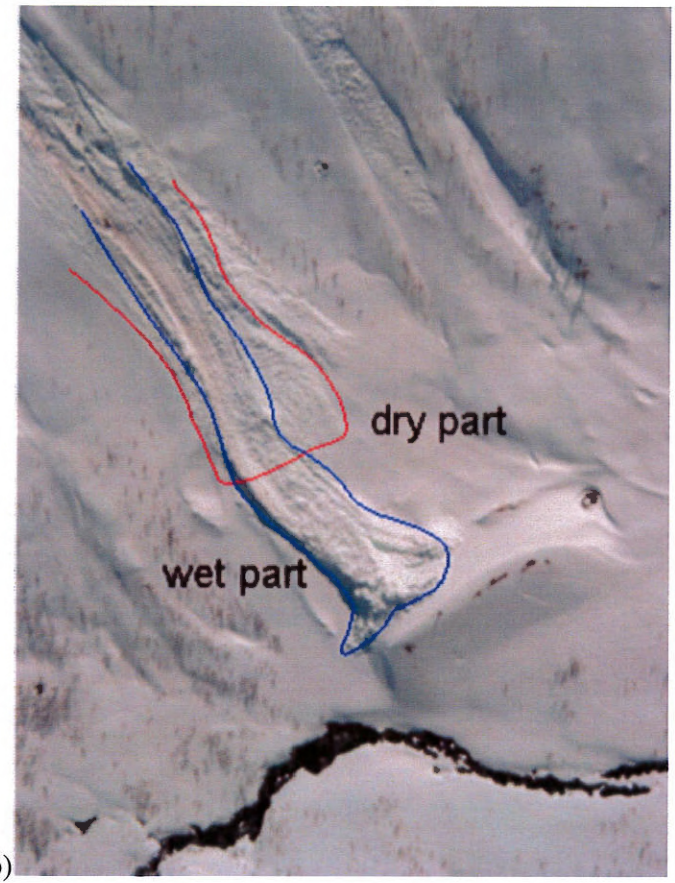

b)

Figure 2.23: Avalanche 20050416 15:00: Deposition/outline map in the Ryggfonn area (upper panel); Avalanche deposit (lower panel; photo by Arne Moe taken from the ridge) The deposits on the right hand side and the outreach pointing to the right origin from previous events.

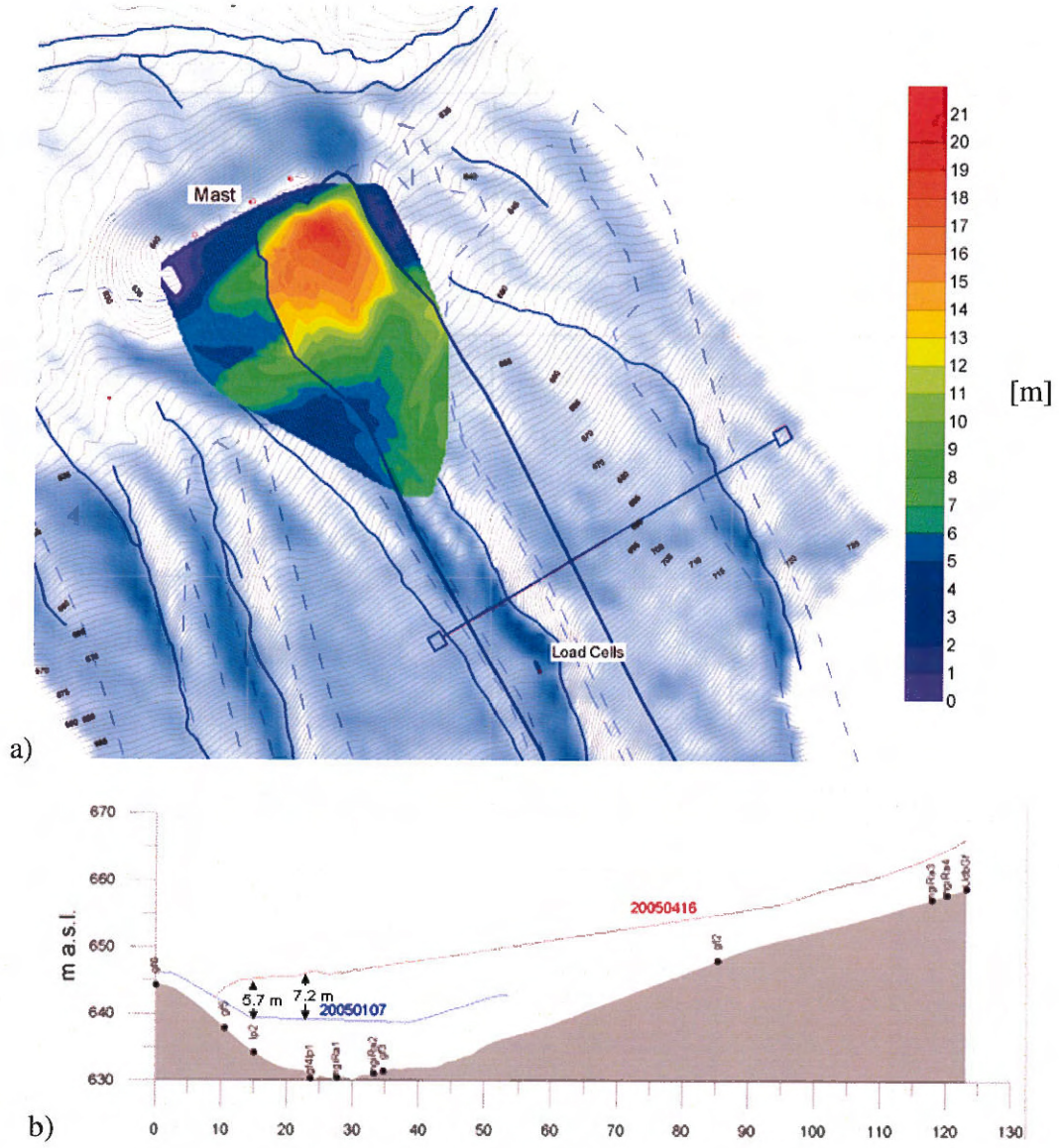

Figure 2.24: Avalanche 20050416 15:00: a) Total deposition in the runout area; b) cross section along the line connecting the load plates

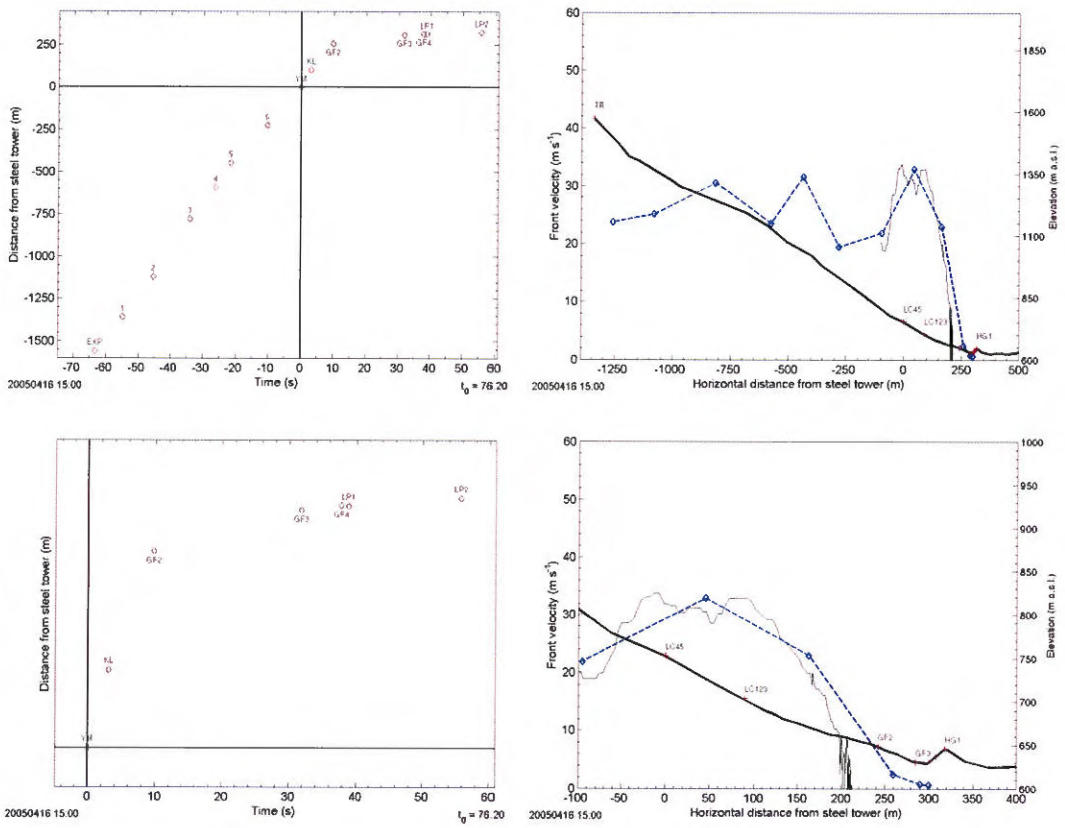

Figure 2.25: Avalanche 20050416 15:00: Timing; Distance vs. time (left); Front velocity vs. horizontal distance (right). Shown are estimates based on the arrival times at various sensor locations and on video analysis. In addition, the thin black line (right side) shows the front velocity measured by the pulsed Doppler radar. Top row shows the whole track whereas the bottom row is an enlargement of the runout area.

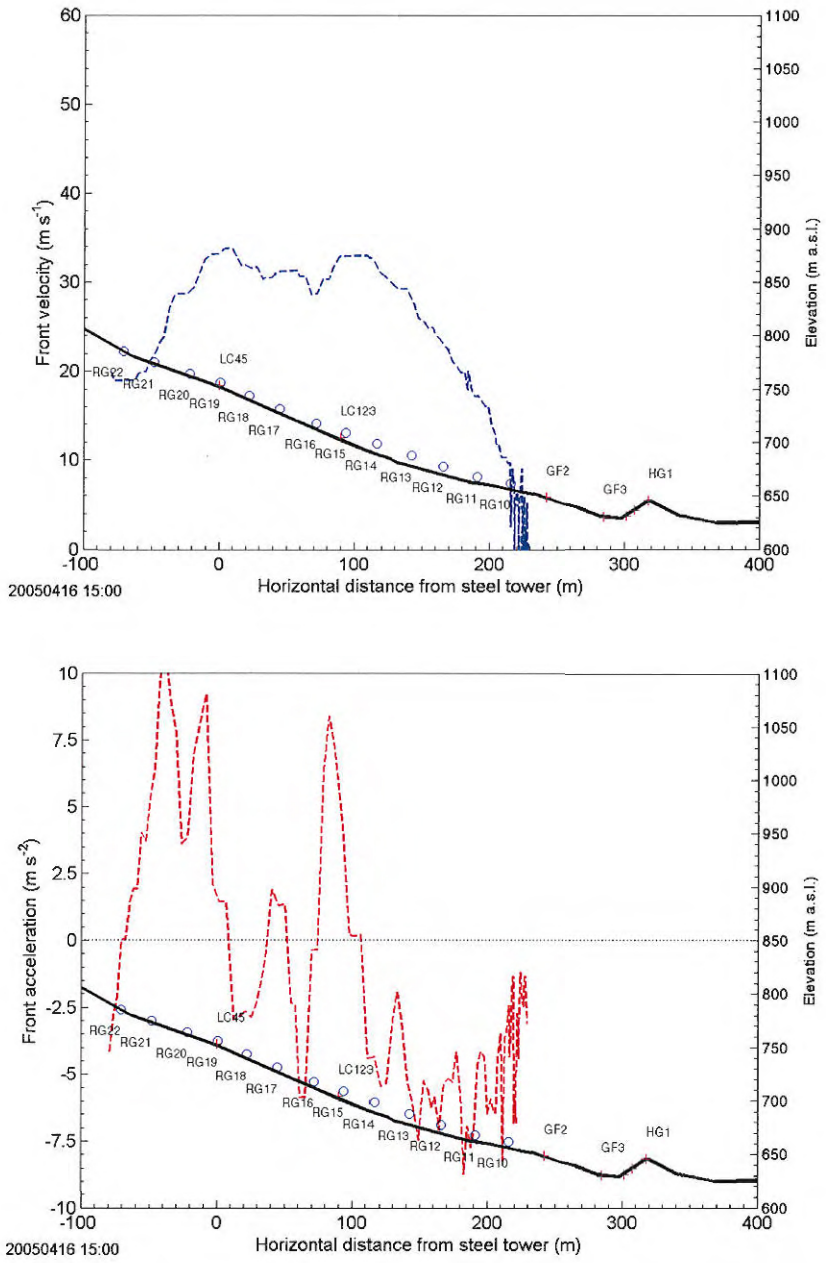

Figure 2.26: Avalanche 20050416 15:00: Front velocity and front acceleration vs. location along the lower track. The upper panel shows the velocity and the lower panel the acceleration derived from the front velocity readings. The thick solid line gives the path profile in the lower part of the track. os indicate the approximated midpoint of the range gate.

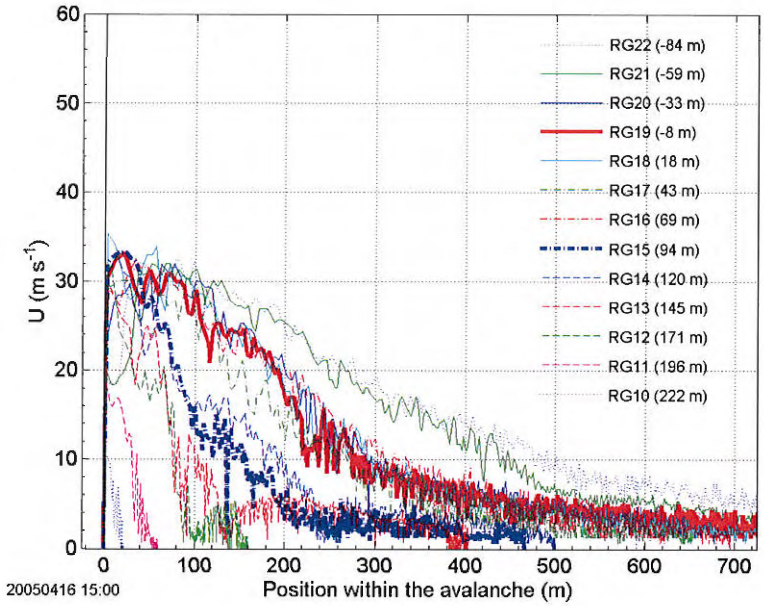

Figure 2.27: Avalanche 20050416 15:00: Velocity vs. position within the avalanche. Shown are all available range gate data.

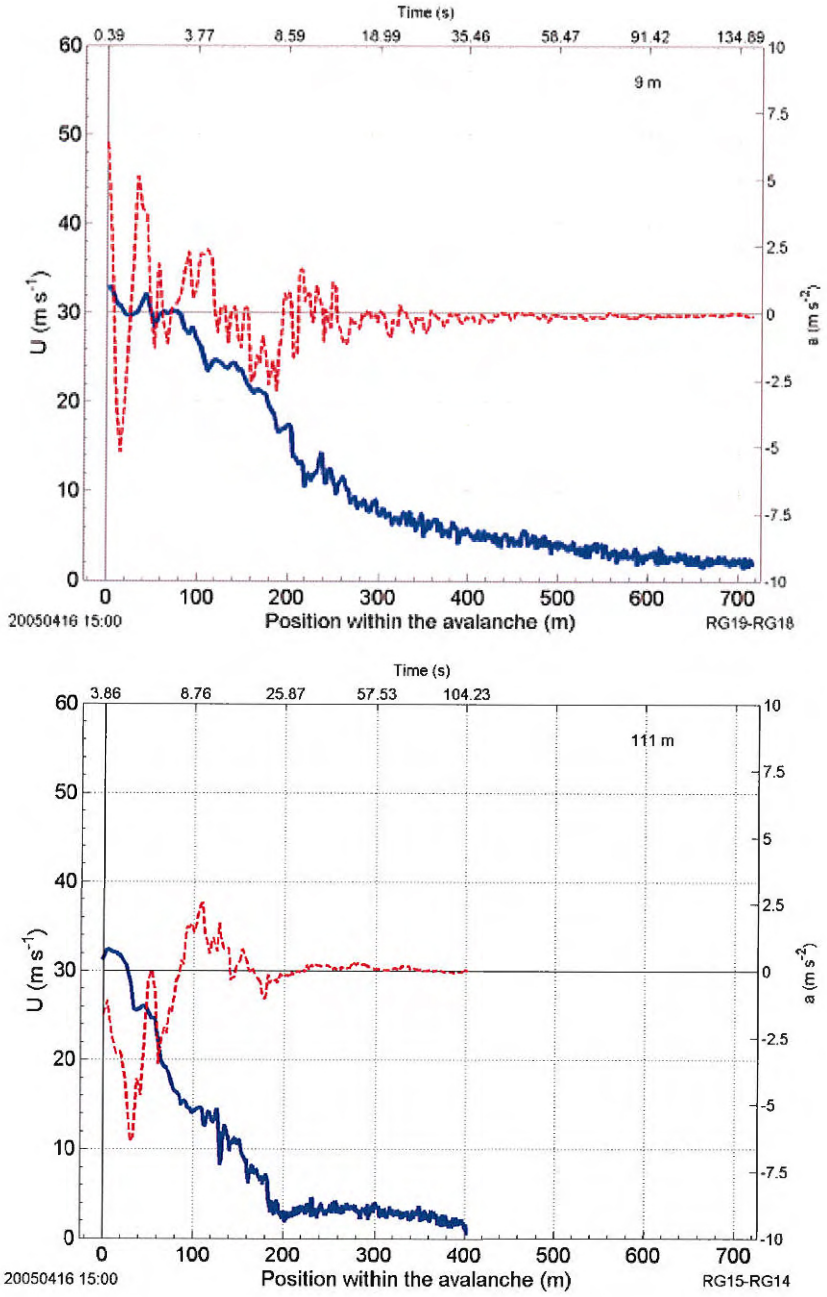

Figure 2.28: Avalanche 20050416 15:00: Velocity (solid line; left ordinate) and acceleration (dashed line; right ordinate) vs. position within the avalanche. Top) values are calculated for a location approximately 9 m below the steel tower (between RG19 and RG18); bottom) values given a point around the concrete wedge (between RG15 and RG14). The mean slope angle at the steel tower is approximately 30° *and at the concrete wedge about* 26°.

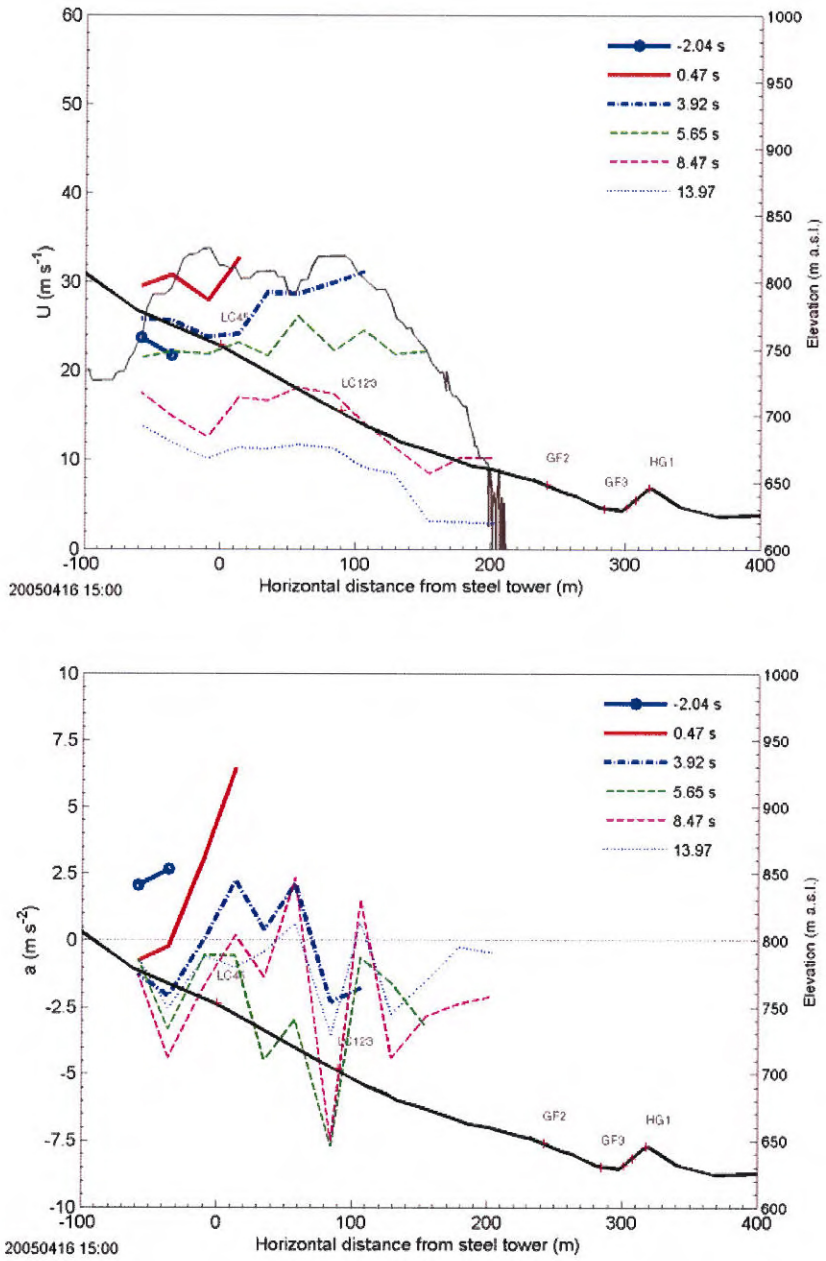

Figure 2.29: Avalanche 20050416 15:00: Velocity and acceleration vs. location along the lower track for six instants in time. The upper panel shows the averaged velocity and the lower panel the acceleration derived from the respective pair of adjoining range gates of the Doppler radar. In addition, the thin solid line in the upper panel shows the front velocity. The thick solid line gives the path profile in the lower part of the track.

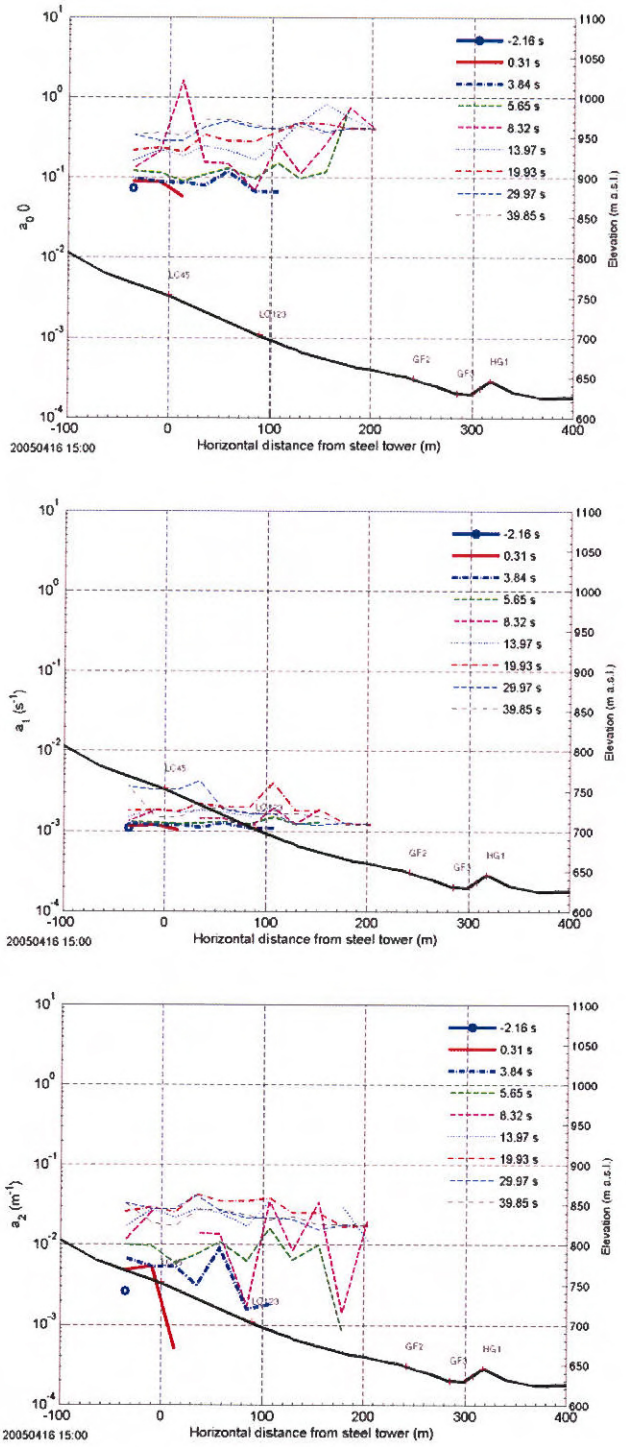

Figure 2.30: Avalanche 20050416 15:00: Friction coefficients (according to (1.8) vs. location along the lower track for nine instants in time. The thick solid line gives the path profile in the lower part of the track.

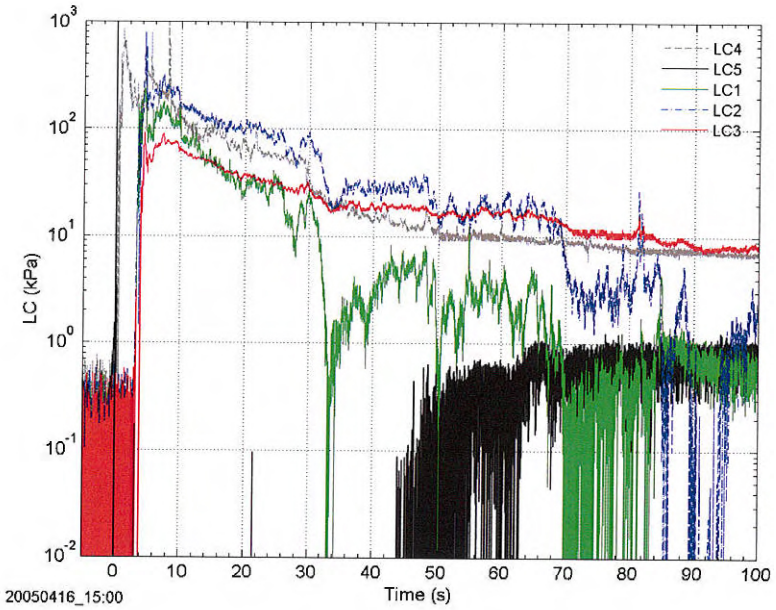

a)

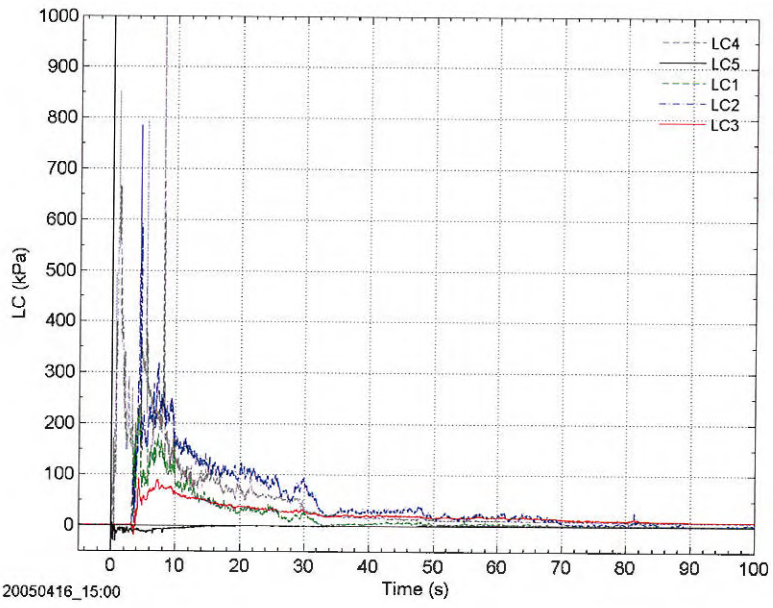

b)

Figure 2.31: Avalanche 20050416 15:00: Load cell measurements: pressure vs. time (raw data; offset corrected); a) logarithmic and b) linear presentation.

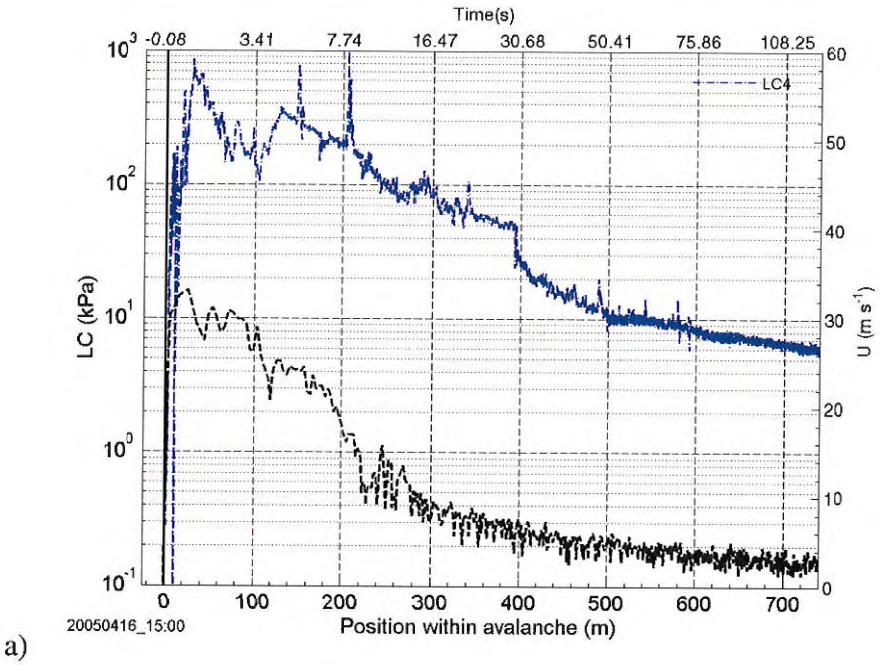

a)

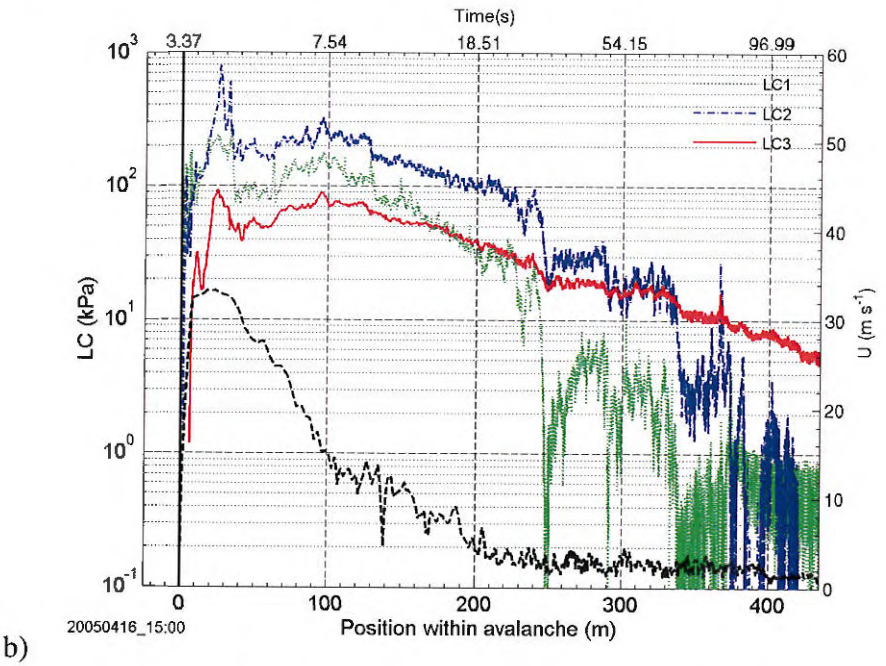

b)

Figure 2.32: Avalanche 20050416 15:00: Load cell measurements: pressure vs. position within the avalanche; a) at steel tower and b) at the concrete wedge. Note the logarithmic scaling of the left ordinate and the different horizontal scaling. The black dashed lines show the corresponding velocity profiles.

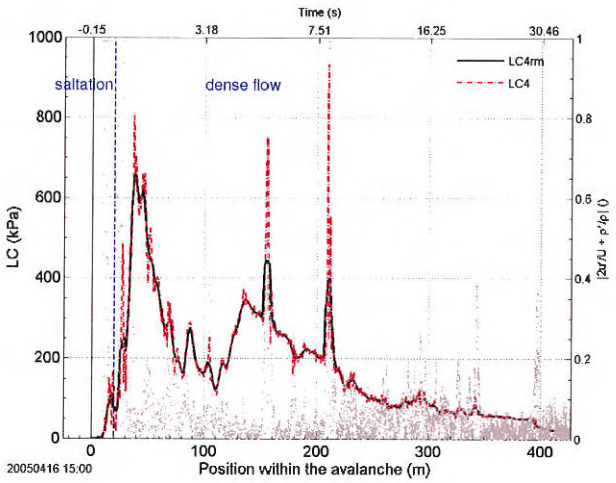

Figure 2.33: Avalanche 20050416 15:00: Fluctuation intensity vs. position within the avalanche. The lines present the measured impact pressure (dashed line) and the running mean (full line) taken over 5 m, respectively (left axis), at the concrete wedge. The fluctuation intensity is marked with dots (right axis). LC4 (LC5 was partly buried at the time).

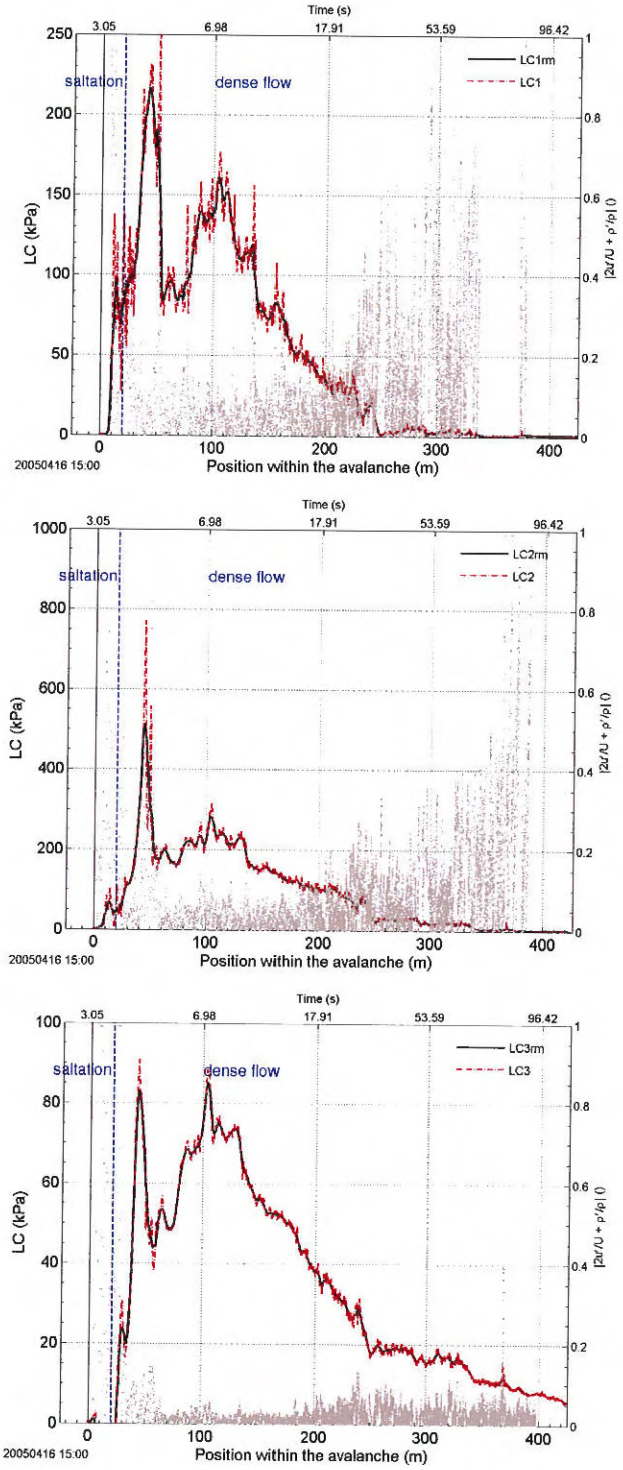

Figure 2.34: Avalanche 20050416 15:00: Fluctuation intensity vs. position within the avalanche. The lines present the measured impact pressures (dashed line) and the running means (full line) taken over 5 m, respectively (left axis), at the concrete wedge. The fluctuation intensities is marked with dots (right axis). Top: LC1; middle: LC2; bottom LC3 (partly buried at the time).

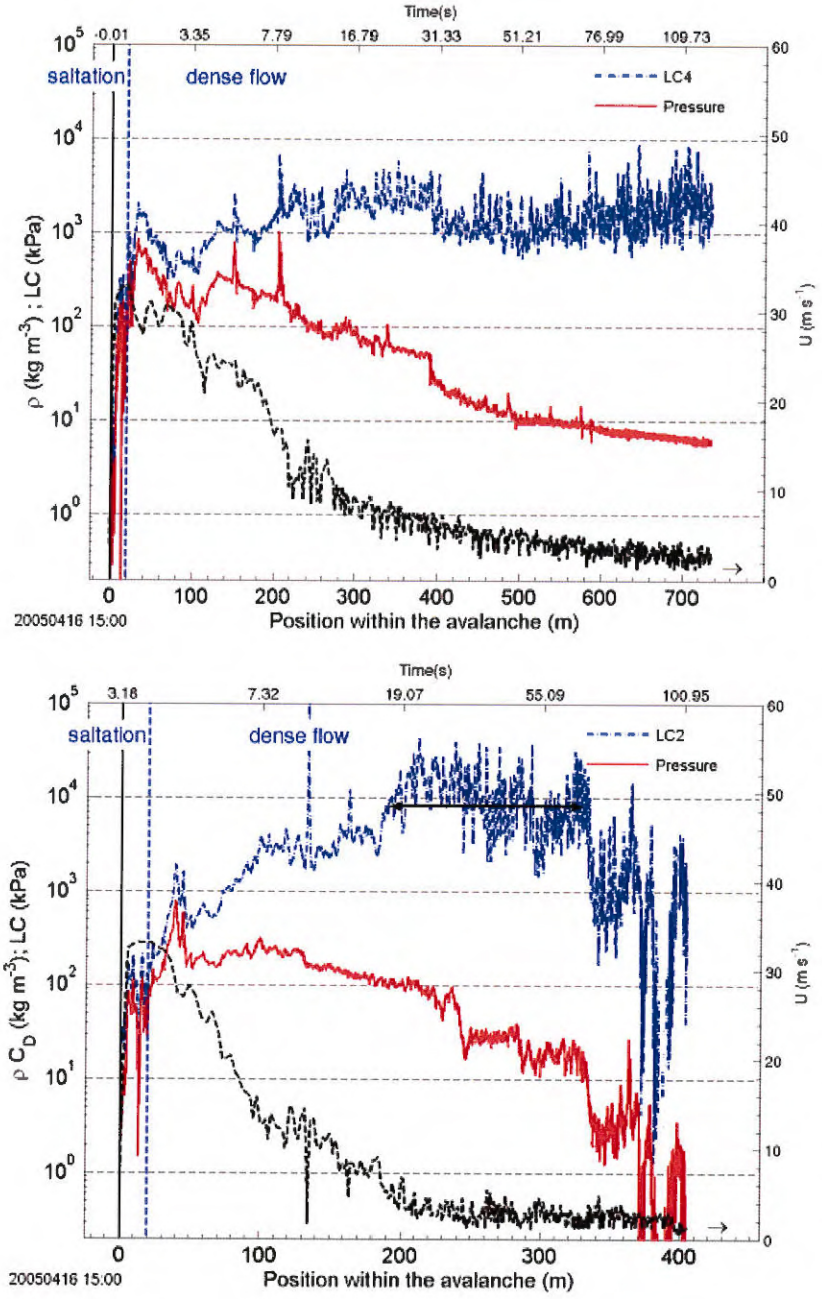

Figure 2.35: Avalanche 20050416 15:00: ρC_D vs. position within the avalanche (dash-dotted line). The full lines represent the measured impact pressure as the running mean taken over 5 m. Note the logarithmic scaling of the left ordinate and the different horizontal scaling. The black dashed lines show the corresponding velocity profiles. Upper panel gives measurements from the steel tower (LC4) and the lower panel from the concrete wedge (LC2).

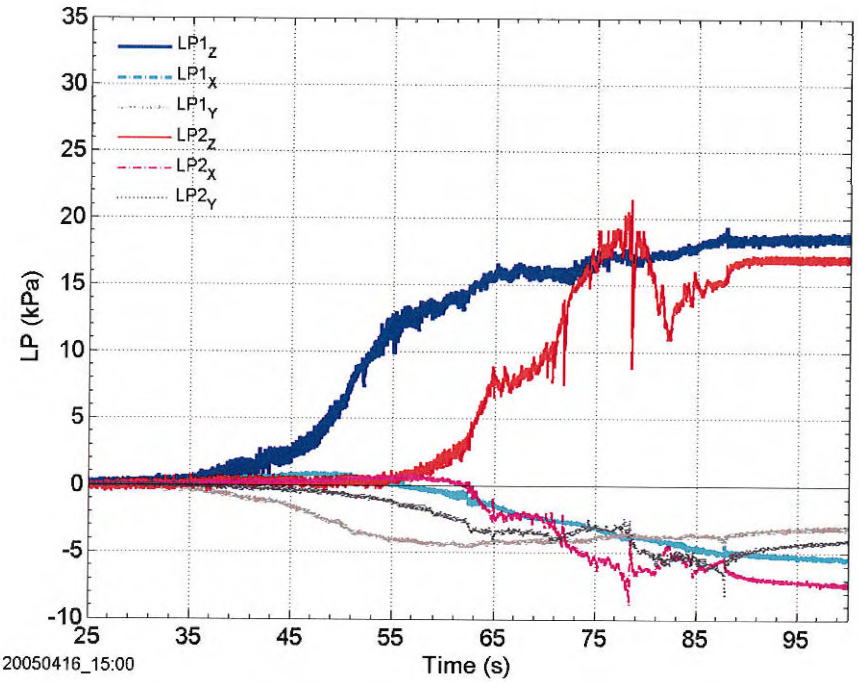

Figure 2.36: Avalanche 20050416 15:00: Load plate measurements: LP (raw data) vs. time.

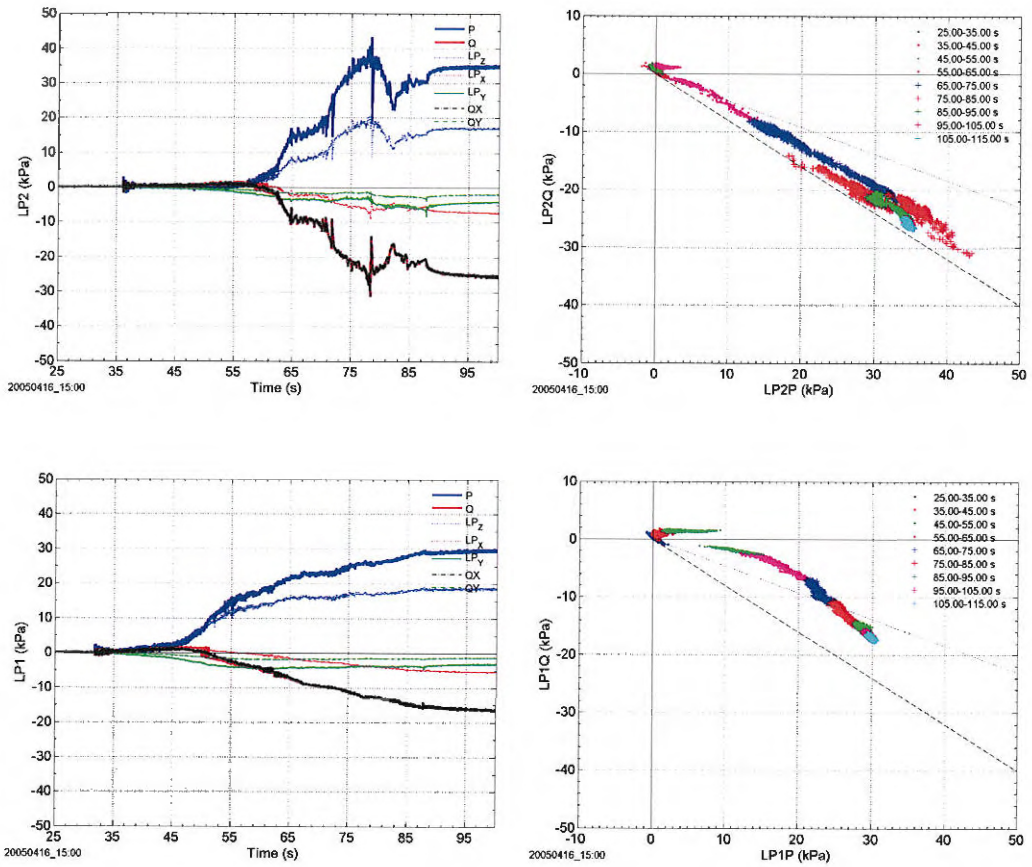

Figure 2.37: Avalanche 20050416 15:00: Load plate measurements: Stresses vs. time (left hand side) and shear stress vs. normal stress at the sliding plane (surface of the snowpack) along the dam slope (right hand side). The upper panel shows LP2 and the lower one LP1. LP_z, LP_x, and LP_y mark the measured stresses. P, Q_x, and Q_y are the calculated stresses according to (1.3). Q is the total traction. The dashed line in the right panels corresponds to the ratio between shear and normal stress in the case of static loading $(-\tan 40°$ *or* $-\tan 20°)$.

Figure 2.38: Avalanche 20050416 15:00: Series of snapshots from the avalanche descent I. Circles indicate flying snow clods.(Photos by Arne Moe)

Figure 2.39: Avalanche 20050416 15:00: Series of snapshots from the avalanche descent II. Photos are taken approximately every 1 s. Obvious are the impacts of clods around the front; some are difficult to see due to the shadow of the cloud. The impinging clods seem to erode the snowpack and to through small clod up into the air. The clods were not obvious until the track steepened beyond the upper plateau. If one combines this observation with observation from flume experiments (see Fig. 2.40) one might get an idea of possible erosion and entrainment mechanisms at the front of the saltation layer. (Photos by Arne Moe)

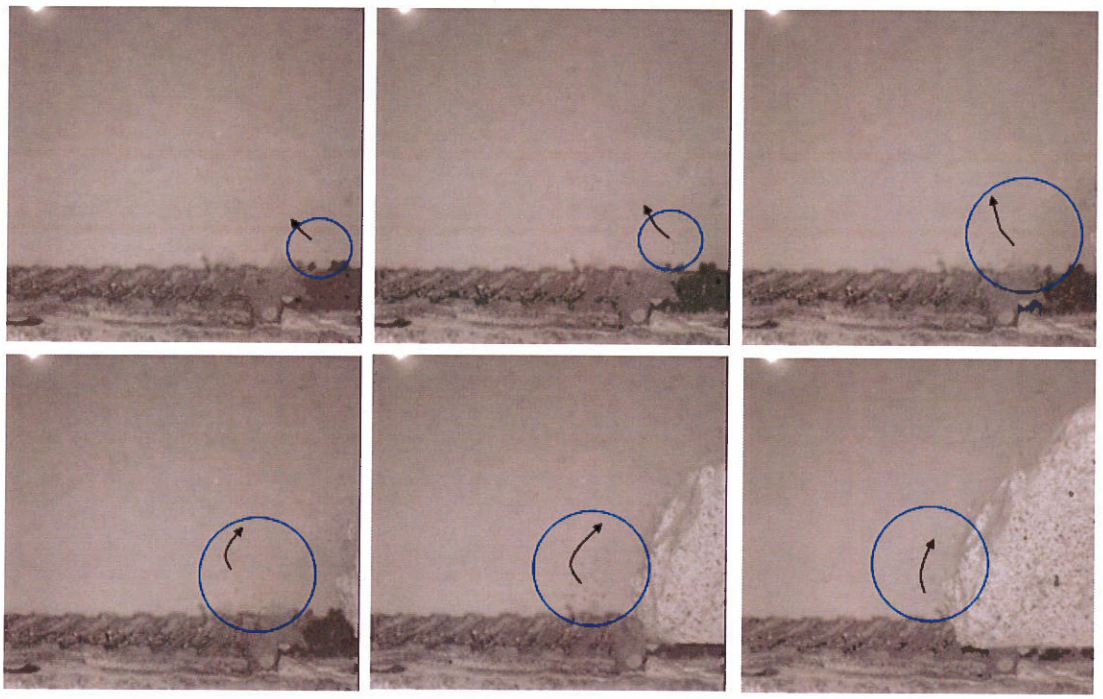

Figure 2.40: Series of snapshots from a subaqueous flume experiment. Photos extracted from a high speed video taken at a fixed position. In this case, the water flow in front of the slide erodes remaining sand and clay particles from a previous experiment. The particles are lifted up (direction indicated by the arrows) and finally incorporated into the slide (video by Trygve Ilstad). The series is included to give an idea of How snow might be incorporated into the flow.

Figure 2.41: Avalanche 20050416 15:00: Snapshots from the track I. Left hand side: during the descent of the avalanche; right hand side after the event (similar location). Obviously, the avalanche eroded during the descent. Scratch marks remind one at erosion/abrasion due to (saltating) particles.(Photos by Arne Moe)

Figure 2.42: Avalanche 20050416 15:00: Snapshots from the track II. Left hand side: Overview; right hand side after the event (Circles indicate similar locations). Obviously, the avalanche eroded during the descent. Scratch marks remind one at erosion/abrasion due to (saltating) particles.(Photos by Karstein lied and Arne Moe)

Figure 2.43: Avalanche 20050416 15:00: Snapshots from the lower track. Line indicates the boundary of the erosion. Inset shows the situation before the release. (Photos by Karstein Lied and Peter Gauer)

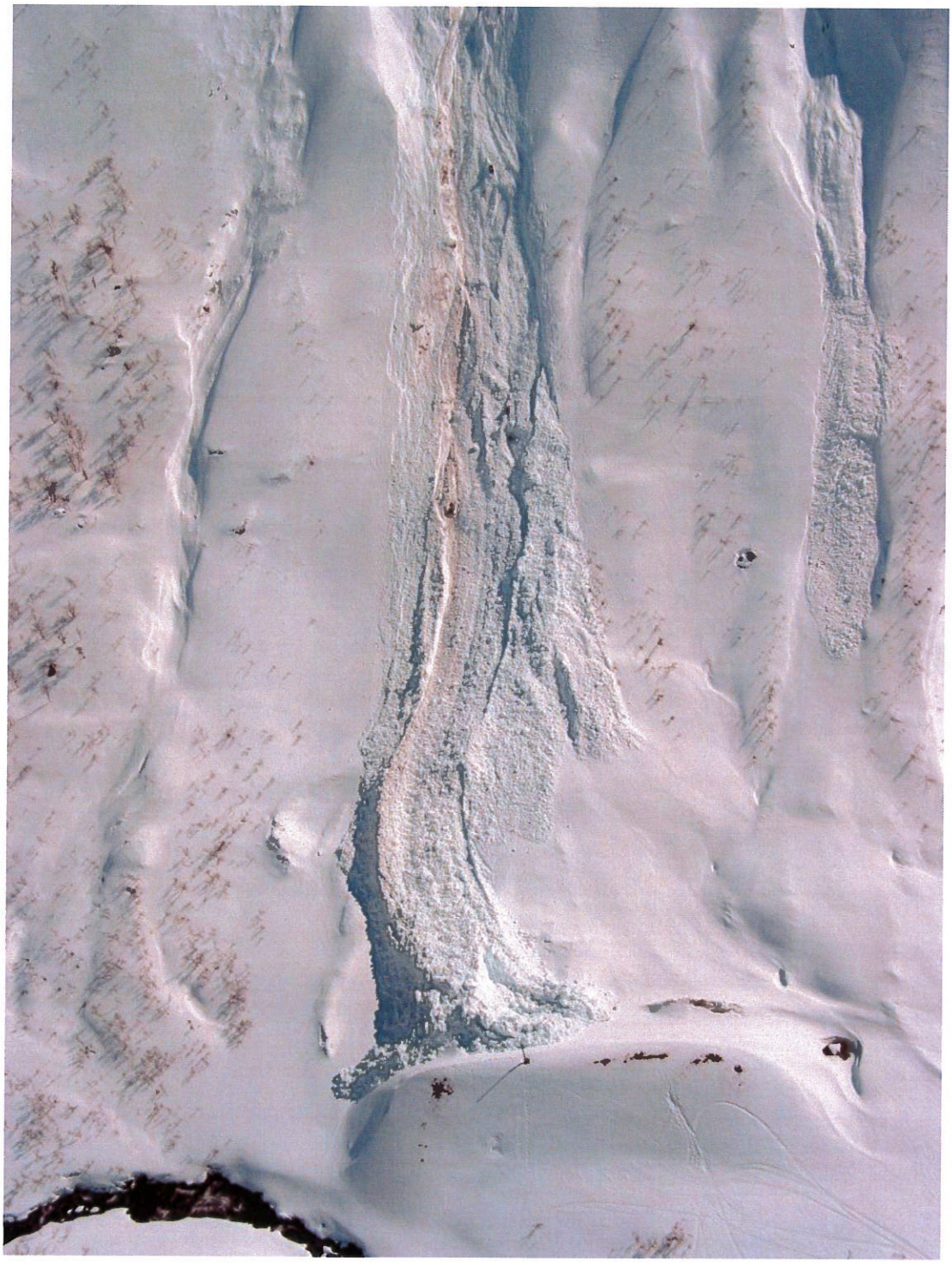

Figure 2.44: Avalanche 20050416 15:00: Snapshots from the lower track (erosion I). One can see a brownish strip indicating erosion of soil. (Photo by Krister Kristensen)

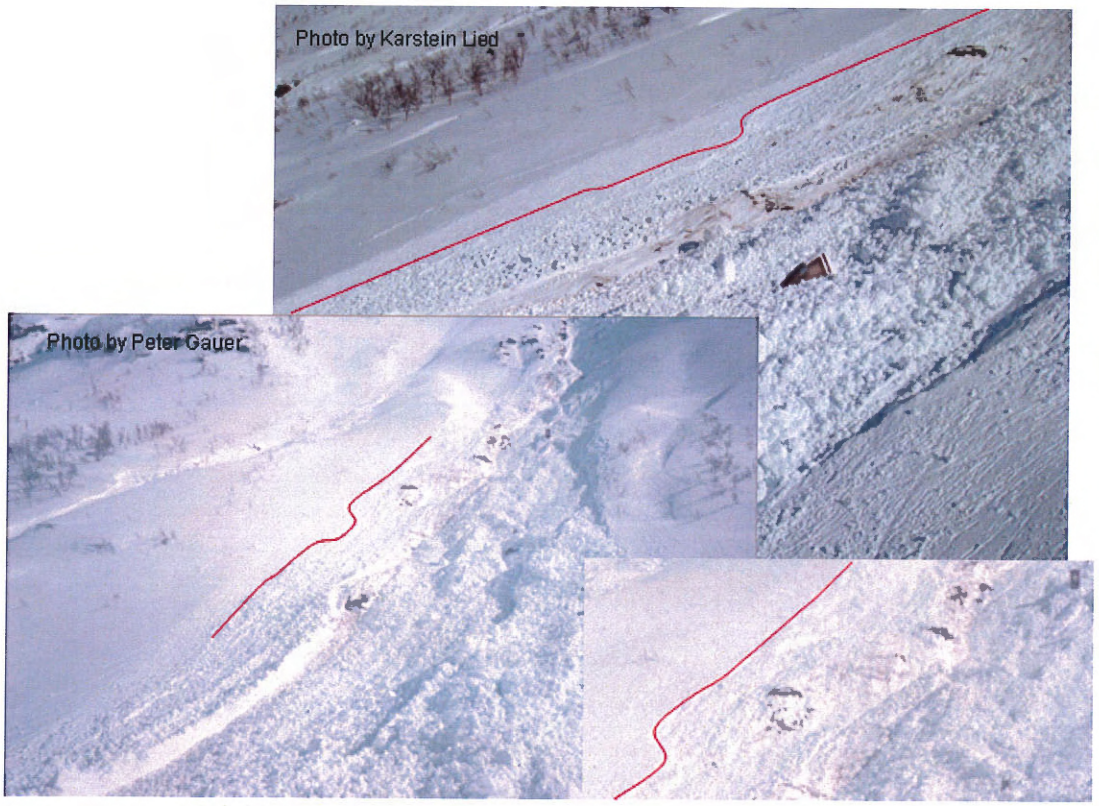

Figure 2.45: Avalanche 20050416 15:00: Snapshots from the lower track (erosion II). Lines indicate the boundary of the erosion. (Photos by Karstein Lied and Peter Gauer)

Figure 2.46: Avalanche 20050416 15:00: Snapshots from the deposits. (Photos by Arne Moe)

References

Johnson, K. L. 2001. *Contact Mechanics*. Cambridge, U.K., Cambridge University Press.

McClung, D. and P. Schaerer. 1993. *The Avalanche Handbook*. 1011 SW Klickitat Way, Seattle, Washington 98134, The Mountaineers.

Mellor, M. 1968. Cold regions science and engineering. Part III: Engeneering, Section A3: Snow Technology Avalanches. Hanover, New Hampshire, Cold Regions Research & Engineering Laboratory.

Norem, H. 1990. Ryggfonn-prosjektet. NGI Report 581200-16. Sognsveien 72, N-0860 Oslo, Norwegian Geotechnical Institute. (in Norwegian).

Salm, B., A. Burkhard, and H. U. Gubler. 1990. Berechnung von Fliesslawinen. eine Anleitung für Praktiker mit Beispielen. Mitt. Eidgenöss. Inst. Schnee- Lawinenforsch. 47. SLF, Davos, Switzerland, 37 pages.

SATSIE, . 2003. *Avalanche Studies and Model Validation in Europe EU: Management Progress Report*. Coordinator: Norwegian Geotechnical Institute, available from http://www.leeds.ac.uk/satsie edition.

Schreiber, H., W. L. Randeu, H. Schaffhauser, and L. Rammer. 2001. Avalanche dynamics measurement by pulsed Doppler radar. *Annals of Glaciology*, **32**, 275–280.

UNESCO, . 1981. *Avalanche Atlas*. International Commission on Snow and Ice of the International Association of Hydrological Sciences, IAHS.

Table A-1: Code for morphological avalanche classification (1981, Avalanche Atlas/UNESCO)

Criterion / Characteristics	Symbols: Criterion	Characteristics: pure	Characteristics: mixed
Manner of starting	A		
Loose snow avalanche		1	7
Slab avalanche		2	7
Slab avalanche soft		3	
Slab avalanche hard		4	
Position of sliding surface	B		
Surface-layer avalanche (general)		1	7
Surface-layer avalanche, new snow fracture		2	8
Surface-layer avalanche, old snow fracture		3	8
Full-depth avalanche		4	7
Liquid Water in snow fracture	C		
Absent: dry-snow avalanche		1	7
Present: wet-snow avalanche		2	7
Form of Path	D		
Unconfined avalanche		1	7
Channelled avalanche		2	7
From of movement	E		
Powder avalanche (dominant)		1	7
Flow avalanche (dominant)		2	7
Surface roughness of deposit	F		
Coarse deposit (general)		1	7
Coarse deposit angular blocks		2	7
Coarse deposit rounded clods		3	7
Fine deposit		4	7
Liquid water in deposit	G		
Absent: dry-deposit		1	7
Present: wet-deposit		2	7
Contamination of deposit	H		
Clean deposit		1	7
Contaminated deposit (general)		2	7
Contaminated by rocks, debris, soil		3	8
Contaminated by branches, trees		4	8
Contaminated by debris of structures		5	
Triggering mechanism[1]	J		
Natural release		1	
Human release (general)		2	
Human release, accidental		3	
Human release, intentional		4	

[1]This criterion is an element of the genetic classification. since the triggering mechanism within the given alternatives is known most cases and is important for many problems, it is added to the morphological code.

Table A-2: Canadian snow avalanche size classification system and typical factors (McClung and Schaerer, 1993)

Size	Description	Typical mass (Mg)	Typical path length (m)	Typical impact pressure (kPa)
1	Relative harmless to people	< 10	10	1
2	Could bury, injure or kill a person	10^2	100	10
3	Could bury a car, destroy a small building, or break a few trees	10^3	1000	100
4	Could destroy a railway car, large truck, several buildings, or a forest with an area up to 4 hectares	10^4	2000	500
5	Largest snow avalanche known; could destroy a village or a forest of 40 hectares	10^5	3000	1000

Kontroll- og referanseside/ *Review and reference page*

Oppdragsgiver/*Client* European Commission **Kontraktsreferanse/** Contract of 18.10.02 ***Contract reference***	**Dokument nr/*Document No.*** 20021048-8 **Dato/*Date*** 2005-12-01
Dokumenttittel/*Document title* Ryggfonn measurements **Prosjektleder/*Project Manager*** Karstein Lied **Utarbeidet av/*Prepared by*** Peter Gauer and Krister Kristensen	**Distribusjon/*Distribution*** ☐ **Fri/*Unlimited*** ☒ **Begrenset/*Limited*** ☐ **Ingen/*None***
Emneord/*Keywords*	
Land, fylke/*Country, County* Norway, **Kommune/*Municipality*** Stryn **Sted/*Location*** Grasdalen, Ryggfonn **Kartblad/*Map*** 1418 IV, Lodalskåpa **UTM-koordinater/*UTM-coordinates*** 32VMP094725	**Havområde/*Offshore area*** **Feltnavn/*Field name*** **Sted/*Location*** **Felt, blokknr./*Field, Block No.***

Kvalitetssikring i henhold til/*Quality assurance according to* NS-EN ISO9001

Kontrollert av/ *Reviewed by*	Kontrolltype/ *Type of review*	Dokument/*Document* Kontrollert/*Reviewed* Dato/*Date*	Sign.	Revisjon 1/*Revision 1* Kontrollert/*Reviewed* Dato/*Date*	Sign.	Revisjon 2/*Revision 2* Kontrollert/*Reviewed* Dato/*Date*	Sign.
KL	Helhetsvurdering/ *General Evaluation* *	22/11-05	KL				
K.L	Språk/*Style*	22/11-05	KL				
KL	Teknisk/*Technical* - Skjønn/*Intelligence* - Total/*Extensive* - Tverrfaglig/ *Interdisciplinary*	22/11-05	KL				
PG	Utforming/*Layout*	22.11.2005					
PG	Slutt/*Final*	22.11.2005					
BPe	Kopiering/*Copy quality*	22/11-05	BPe				

* Gjennomlesning av hele rapporten og skjønnsmessig vurdering av innhold og presentasjonsform/ *On the basis of an overall evaluation of the report, its technical content and form of presentation*

Dokument godkjent for utsendelse/ *Document approved for release*	Dato/*Date* 22.11.2005	Sign.